Neuron

Article

Runx1 transcription factor modulates opioid analgesia and withdrawal in humans and rodents

Highlights

- Runt-related transcription factor (Runx1) modulates microglial reactivity
- Runx1 deletion produces a distinct microglial transcriptional signature
- Runx1 deletion reduces morphine potency and exacerbates opioid withdrawal
- *RUNX1* variants link to perioperative opioid analgesia and withdrawal severity

Authors

Heather Leduc-Pessah, Brendan B. McAllister, Sarthak Sinha, ..., Kazutaka Ikeda, Jeff Biernaskie, Tuan Trang

Correspondence

trangt@ucalgary.ca

In brief

Opioid responses differ across individuals. Runt-related transcription factor 1 (Runx1) modulates the microglial transcriptome, influencing opioid analgesia and withdrawal. *RUNX1* variants may underlie inter-individual differences in opioid responses, guiding personalized strategies to optimize opioid pain management and minimize adverse outcomes.

Leduc-Pessah et al., 2026, Neuron *114*, 1–19
March 4, 2026
https://doi.org/10.1016/j.neuron.2025.11.018

CellPress

Neuron

CellPress

Article

Runx1 transcription factor modulates opioid analgesia and withdrawal in humans and rodents

Heather Leduc-Pessah,[1,2,3] Brendan B. McAllister,[1,2,3] Sarthak Sinha,[1] Sierra Stokes-Heck,[1,2,3] Daisuke Nishizawa,[4,5] Churmy Y. Fan,[1,2,3] Marie-Kim St-Pierre,[6] Amyaouch Bradaia,[2,3,7] Manon Defaye,[2,3,7] Nicole E. Burma,[1,2,3] Jonathan Damblon,[8] Einer Muñoz-Pino,[8] Frank Visser,[3] Marie-France Dorion,[9] Luke M. Healy,[9] Ye Man Tang,[10] Julia Canet-Pons,[1,2,3] Nynke J. van den Hoogen,[1,2,3] Zizhen Zhang,[3,11] Flavia T.T. Antunes,[3,11] Valerio E.C. Piscopo,[10] Margaret Medina,[1,2,3] Ken-ichi Fukuda,[12] Tatsuya Ichinohe,[13] Makoto Nagashima,[14] Masakazu Hayashida,[4,15,16] Emma Johnson,[17] Arpana Agrawal,[17] Louisa Degenhardt,[18] Nicholas G. Martin,[19] Gerald W. Zamponi,[3,11] Elliot C. Nelson,[17] Christophe Altier,[2,3,7] Marie-Eve Tremblay,[6] Chad Bousman,[2,3,20] Stefano Stifani,[10] Yves De Koninck,[8] Kazutaka Ikeda,[4,5] Jeff Biernaskie,[1,3,21] and Tuan Trang[1,2,3,22,*]

[1]Faculty of Veterinary Medicine, University of Calgary, Calgary, AB T2N 4N1, Canada
[2]Department of Physiology & Pharmacology, Cumming School of Medicine, University of Calgary, Calgary, AB T2N 4N1, Canada
[3]Hotchkiss Brain Institute, University of Calgary, Calgary, AB T2N 4N1, Canada
[4]Addictive Substance Project, Tokyo Metropolitan Institute of Medical Science, 2-1-6, Kamikitazawa, Setagaya-ku, Tokyo 156-8506, Japan
[5]Department of Neuropsychopharmacology, National Institute of Mental Health, National Center of Neurology and Psychiatry, Kodaira, Tokyo, Japan
[6]School of Medical Sciences, University of Victoria, Victoria, BC, Canada
[7]Snyder Institute for Chronic Diseases, University of Calgary, Calgary, AB T2N 4N1, Canada
[8]CERVO Brain Research Centre, Québec Mental Health Institute, Graduate program in Neuroscience, Université Laval University, Department of Psychiatry and Neuroscience, Department of Anesthesiology & Intensive Care, Université Laval, Quebec City, QC, Canada
[9]Neuroimmunology Unit, Montreal Neurological Institute, McGill University, Montreal, QC, Canada
[10]Department of Neurology and Neurosurgery, Montreal Neurological Institute-Hospital, McGill University, Montreal, QC, Canada
[11]Department of Clinical Neurosciences, University of Calgary, Calgary, AB, T2N RN1, Canada
[12]Department of Oral Health and Clinical Science, Tokyo Dental College, 2-9-18, Misaki-cho, Chiyoda-ku, Tokyo 101-0061, Japan
[13]Department of Dental Anesthesiology, Tokyo Dental College, 2-9-18, Misaki-cho, Chiyoda-ku, Tokyo 101-0061, Japan
[14]Department of Surgery, Toho University Sakura Medical Center, 564-1, Shimoshizu, Sakura-shi, Chiba 285-8741, Japan
[15]Department of Anesthesiology, Saitama Medical University International Medical Center, 1397-1, Yamane, Hidaka, Saitama 350-1298, Japan
[16]Department of Anesthesiology and Pain Medicine, Juntendo University School of Medicine, 2-1-1, Hongou, Bunkyou-ku, Tokyo 113-8421, Japan
[17]Department of Psychiatry, Washington University School of Medicine, St. Louis, MO, USA
[18]National Drug and Alcohol Research Centre, University of New South Wales, Sydney, NSW, Australia
[19]QIMR Berghofer Medical Research Institute, Brisbane, QLD, Australia
[20]Department of Medical Genetics, and Department of Psychiatry, University of Calgary, Calgary, AB, Canada
[21]Department of Surgery, Cumming School of Medicine, University of Calgary, Calgary, AB T2N 4N1, Canada
[22]Lead contact
*Correspondence: trangt@ucalgary.ca
https://doi.org/10.1016/j.neuron.2025.11.018

SUMMARY

Opioid analgesia and adverse outcomes vary across individuals. We show that runt-related transcription factor 1 (Runx1) modulates the microglial transcriptome and is a genetic determinant of opioid antinociceptive responses and withdrawal. In mice, Runx1 deletion in microglia produces distinct ultrastructural and transcriptomic signatures, reducing morphine potency despite no prior opioid exposure. These mice also require greater post-operative morphine and display exacerbated morphine-induced hyperalgesia and withdrawal. Single-cell RNA sequencing (scRNA-seq) and chromatin immunoprecipitation sequencing (ChIP-seq) analyses reveal a unique microglial state, with Runx1 regulating inflammatory signaling and key microglial functions. In humans, association analyses link *RUNX1* variants to inter-individual differences in perioperative opioid requirement and withdrawal severity. Identifying *RUNX1* susceptibility genotypes may be important for understanding individual variability in opioid responses, with potential relevance for future personalized approaches.

Please cite this article in press as: Leduc-Pessah et al., Runx1 transcription factor modulates opioid analgesia and withdrawal in humans and rodents, Neuron (2025), https://doi.org/10.1016/j.neuron.2025.11.018

INTRODUCTION

Opioid medications are widely used to treat pain and are particularly effective in managing acute, short-term pain conditions.[1–3] However, both their analgesic and adverse effects vary considerably across individuals.[4–7] Prolonged opioid use, in particular, can differentially increase the risk of opioid dependence, analgesic tolerance, and opioid-induced hyperalgesia.[1,8–11] These inter-individual differences underscore the need to understand the cellular and molecular mechanisms of opioid action and to identify genetic variants that may help predict which patients are most likely to benefit from opioid therapy.[12–15]

Chronic opioid treatment promotes a shift in microglia toward a reactive phenotype.[16–18] This shift is characterized by changes in morphology, release of proinflammatory cytokines, and altered gene expression.[9,19,20] Opioids are proposed to influence microglial responses through μ-receptor[17,21–23] and μ-receptor-independent[24–26] mechanisms that activate a variety of signaling pathways linked to many adverse consequences of chronic opioid use.[9,26,27] Since microglial reactivity and phenotypic diversification are transcriptionally controlled, we asked whether transcriptional regulation is a key modulator of microglial response to opioid exposure. Several transcription factors influence microglial reactivity, including the activator protein-1 (AP1) transcription factor subunit (Jun), interferon regulatory factor 8 (IRF8), musculoaponeurotic fibrosarcoma oncogene homolog B (MafB), myocyte enhancer factor 2A (Mef2A), Mef2C, Spalt-like (Sall1), PU.1, and runt-related transcription factor 1 (Runx1).[28–34] However, the therapeutic implications of this transcriptional regulation are poorly defined. Here, we show that Runx1 modulates opioid responses in rodents and humans. In mice, conditional knockout of *Runx1* in microglia alters both ultrastructure and transcriptional profiles, promoting a reactive state while reducing opioid analgesic efficacy and exacerbating adverse effects. In humans, we identify an important association between *RUNX1* and individual variability in opioid responses.

RESULTS

Runx1 inhibition induces a reactive microglial phenotype and reduces morphine antinociception

We first asked whether repeated opioid exposure affects the expression of transcription factors known to modulate microglial reactivity.[28–34] BV2 microglia-like cells were exposed to morphine or saline in culture for 5 days, and qPCR analysis of these cells revealed that morphine downregulated transcripts of *Runx1* (Figure 1A) and *Spi1* (PU.1) (Figure S1A) but did not affect *Jun*, *Irf8*, *MafB*, *Mef2A*, *Mef2C*, or *Sall1* (Figures S1B–S1G). The reduction in transcripts was concomitant with lower Runx1 protein levels (Figure 1B), whereas PU.1 protein was not affected by repeated morphine treatment (Figure S1H). Likewise, in rat primary microglial culture, morphine downregulated Runx1 protein (Figure 1C).

Runx1 is a transcriptional repressor of microglial reactivity, modulating microglial differentiation and functional state by suppressing the proliferation of amoeboid microglia and promoting ramified morphologies.[29,32,35,36] To inhibit Runx1, we used Ro5-3335 (Ro5; 0.5 μM), which prevents interaction of Runx1 with core-binding factor β (CBFβ), and this interaction is critical for Runx1 transcriptional activity (Figure 1D).[37] Application of Ro5 upregulated the mitotic cell marker Ki67 in primary microglia (Figure S2A) and increased transcript levels of CD11b, CD68, and CD206 in BV2 cells (Figures S2B–S2D). We also detected elevated cytokine release in BV2 cells treated with Ro5 (Figure S2E), indicating that Runx1 inhibition induces a reactive microglial state with a greater propensity to proliferate and secrete proinflammatory cytokines.

We next examined the *in vivo* effects of Ro5 on morphine antinociceptive responses. Adult male Sprague Dawley rats given intrathecal Ro5 (15 μg) or saline displayed comparable tail-flick latencies (Ro5: 3.1 ± 0.26 s, saline 2.7 ± 0.05 s, $p = 0.0549$), indicating that spinal Runx1 inhibition did not alter baseline thermal nociceptive threshold. Moreover, Runx1 within the spinal dorsal horn is localized in microglia,[29,32] and intrathecal Ro5 treatment increased spinal microglial reactivity (Figures 1E–1G). Intrathecal Ro5 also diminished the antinociceptive response to an acute injection of morphine (15 mg/kg intraperitoneally [i.p.]) (Figures 1H and 1I). Reduced antinociceptive potency was confirmed by a rightward shift in morphine dose-response and increased median effective dose (ED_{50}) (Figure 1J). A similar attenuation of morphine antinociception was observed in female rats treated with intrathecal Ro5 (Figure S2F). In the hot plate test, which assesses supraspinal nociceptive responses, intrathecal Ro5 injections also diminished morphine (10 mg/kg i.p.) antinociception in both male and female rats as compared with saline controls (Figures S2G and S2H). These findings indicate that spinal Runx1 inhibition blunts morphine antinociception, despite normal nociceptive thresholds and no prior opioid exposure.

Deletion of *Runx1* in microglia induces ultrastructural and transcriptomic changes

To target Runx1 in microglia, we generated mice with a tamoxifen-inducible deletion of *Runx1* in cells expressing the CX3 chemokine receptor 1 (*Cx3cr1*-Cre^{ERT2}::*Runx1*$^{flx/flx}$) (Figure S3A). Within the lumbar spinal cord of these mice, we confirmed that the Cre^{ERT2} reporter enhanced yellow fluorescent protein (EYFP) was localized to CD11b-positive cells (Figure S3B) and that tamoxifen administration caused Cre recombination (Figure S3C).[38] To allow for the repopulation of peripheral, but not central, CX_3CR_1-expressing cells, experiments were performed 28 days after tamoxifen injections (Figure S3D).[38–40] At this time point, the number of Runx1/CD11b co-stained cells was markedly reduced in the spinal cord of tamoxifen-treated *Cx3cr1*-Cre^{ERT2}::*Runx1*$^{flx/flx}$ mice (Figure S3E). Decreased Runx1/CD11b co-staining was not observed in tamoxifen-injected mice lacking inducible Cre (*Runx1*$^{flx/flx}$) (Figure S3E). As an additional validation, we used fluorescence-activated cell sorting (FACS) to isolate spinal CD11b-positive cells from tamoxifen-treated *Cx3cr1*-Cre^{ERT2}::*Runx1*$^{flx/flx}$ mice and confirmed that Runx1 transcript was depleted in these cells as compared with CD11b-positive cells from vehicle-treated littermate controls (Figure S3F). In addition, we found that spinal microglial reactivity/proliferation was increased in Runx1-deficient mice, which displayed greater CD11b and Ki67 immunoreactivity (Figures 2A–2C). Electron microscopy analysis revealed ultrastructural changes in spinal Runx1-deficient microglia consistent with a reactive state, including increased microglial density (Figure 2D)

Please cite this article in press as: Leduc-Pessah et al., Runx1 transcription factor modulates opioid analgesia and withdrawal in humans and rodents, Neuron (2025), https://doi.org/10.1016/j.neuron.2025.11.018

CellPress

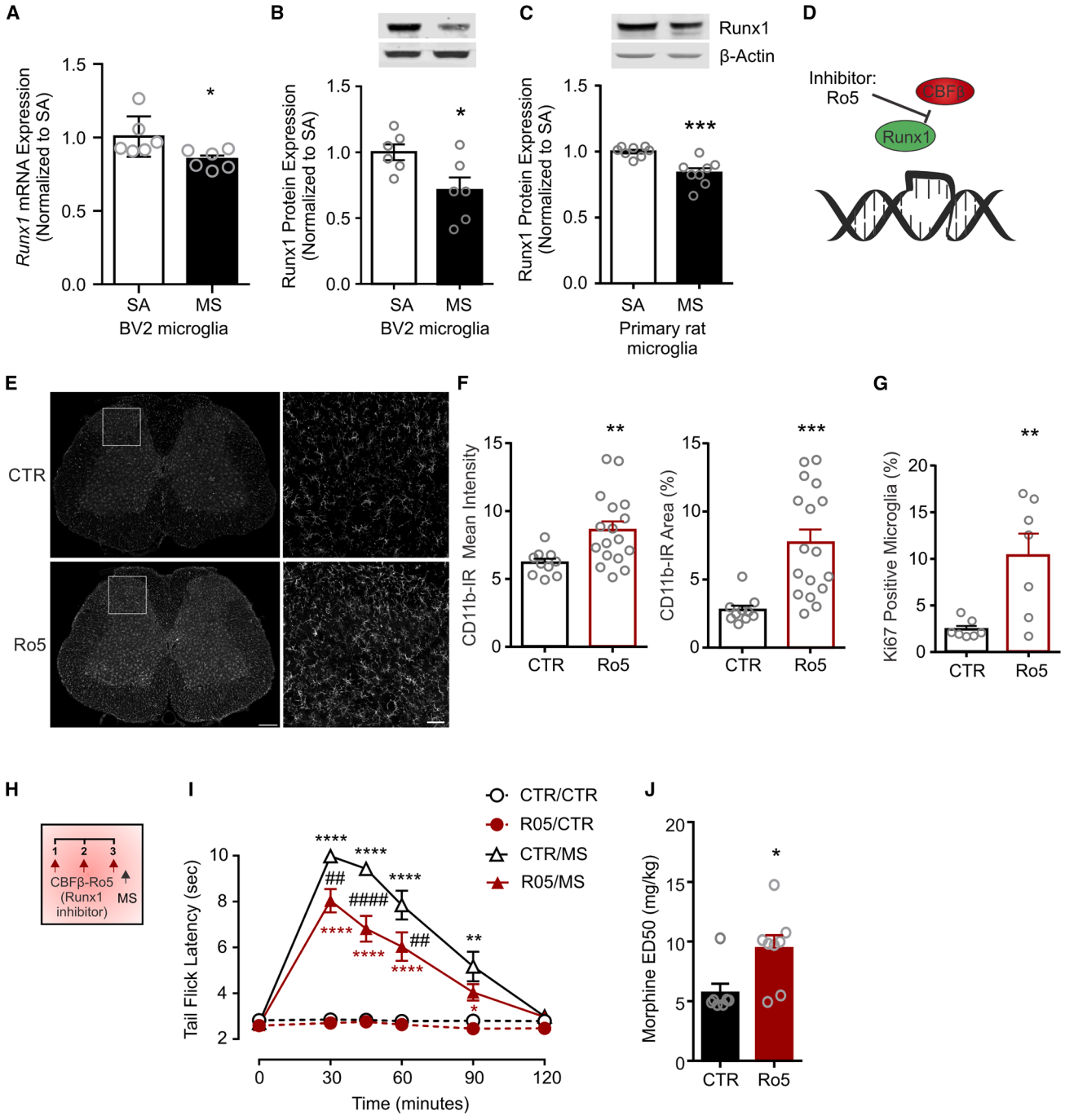

Figure 1. Runx1 inhibition reduces the analgesic potency of morphine

(A–C) BV2 or primary cultured microglia were treated for 5 days with morphine sulfate (MS, 10 μM) or saline (SA). (A) *Runx1* mRNA, normalized to *Rplp1* and expressed relative to SA, from BV2 microglia (unpaired two-tailed *t* test $p = 0.0308$, t = 2.512, df = 10). Runx1 protein, normalized to β-actin and expressed relative to SA, from (B) BV2 (unpaired two-tailed *t* test $p = 0.0308$, t = 2.512, df = 10) and (C) primary microglia (unpaired two-tailed *t* test $p = 0.0007$, t = 4.313, df = 14).

(D) Ro5-3335 (Ro5) interferes with assembly of the Runx1-CBFβ complex on the promoter region of DNA.

(E) Representative images of CD11b expression in the lumbar spinal cord following 3 days of Ro5 or vehicle control (CTR) intrathecal injections (images acquired at 20×, scale bar: 250 μm [left], 50 μm [right]).

(F) Mean intensity of CD11b immunoreactivity (IR) and percent of total area in spinal dorsal horn (CTR, *n* = 10 sections from 2 animals; Ro5, *n* = 17 sections from 3 animals). Unpaired two-tailed *t* test (intensity: $p = 0.0097$, t = 2.8, df = 25; area: $p = 0.0007$, t = 3.9, df = 25).

(G) Percent of CD11b-positive microglia expressing the proliferation marker Ki67 (CTR, *n* = 7 sections from 2 animals; Ro5, *n* = 7 sections from 3 animals). Unpaired two-tailed *t* test ($p = 0.0059$, t = 3.3, df = 12).

(legend continued on next page)

Please cite this article in press as: Leduc-Pessah et al., Runx1 transcription factor modulates opioid analgesia and withdrawal in humans and rodents, Neuron (2025), https://doi.org/10.1016/j.neuron.2025.11.018

and a higher number of lipid bodies per cell (Figures 2E and 2F), as well as reduced microglial cell body circularity and decreased contacts with presynaptic elements (Figures 2G–2L).

To determine whether the ultrastructural changes in Runx1-deficient microglia are concomitant with transcriptomic alterations, we performed single-cell RNA sequencing (scRNA-seq) on FACS-isolated CX_3CR_1-expressing cells from *Cx3cr1*-Cre^{ERT2}::*Runx1*$^{flx/flx}$ mice treated with vehicle (Runx1-expressing) or tamoxifen (Runx1-deficient). Although EYFP expression was observed in mural (Rgs5$^+$Acta2$^+$; 4.6%) and endothelial (Pecam1$^+$Flt1$^+$; 44.0%) cells, active *Cx3cr1* transcripts were exclusive to spinal microglia (Csf1r$^+$Cx3cr1$^+$; 50.0%) (Figures 3A and 3B). Runx1-expressing and Runx1-deficient cells were distributed across all EYFP+ cell clusters. Comparison of global transcriptomic changes across cell populations following Runx1 deletion revealed the greatest perturbation in microglia (Figures 3C and S4A–S4E). Sub-clustering of microglia revealed four unique microglial states: cluster 0 (Cd83, Cxcl2, Ifrd1, tumor necrosis factor [TNF], and Nfkbia), cluster 1 (Olfml3, Rgs1, Serpine2, Klf2, and Tsc22d1), cluster 2 (Basp1, Cx3cr1, Hspa1b, Hk2, and Zfhx3), and cluster 3 (Cfp, Vsp8, Hspa1a, Crybb1, and P2ry12) (Figures 3D–3F). Notably, Runx1 deletion resulted in a depletion of cluster 1 and the concomitant emergence of a unique microglial state characterized by cluster 3. Differential gene expression analysis revealed that of the 16,513 genes detected in microglia, 521 were downregulated and 215 were upregulated in Runx1-deficient microglia relative to Runx1-expressing microglia (http://www.biernaskielab.ca/Runx1_Microglia/) (Figure 3G; Table S1). To assess the functional implications, the top 100 upregulated and downregulated genes were analyzed using Ingenuity Pathway Analysis (IPA; Qiagen) (Figure 3H). Notably, cytokine signaling was affected, with predicted interleukin (IL)-10 inhibition and activation of the IL-6, TNFR1, and TNFR2 pathways. Pathways related to macrophage activity were also implicated, with predicted activation of processes involving nitric oxide and reactive oxygen species production, as well as pathways associated with rheumatoid arthritis. Our findings indicate that depleting Runx1 induces a distinct cellular and transcriptomic profile, consistent with a reactive microglial state.

To identify Runx1's direct binding sites and their corresponding downstream regulons, we performed chromatin immunoprecipitation sequencing (ChIP-seq) on spinal cord homogenate and integrated this analysis with the differentially expressed genes (DEGs) identified from Runx1-deficient microglia by scRNA-seq. ChIP-seq revealed 1,529 Runx1 binding peaks in 83.1% promoter, 6.7% intron, and 8.4% intergenic regions (Figures 4A–4C; Table S1). To validate our ChIP-seq results, we selected several of these genes, as well as *Cdkn1a*, a known Runx1 binding target in microglia,[29] and performed ChIP-qPCR on chromatin isolated from cultured primary microglia, using primers targeting the predicted Runx1 binding sites. We observed greater IP with Runx1 antibody relative to control rabbit immunoglobulin G (IgG) (Figures S4F–S4I), confirming that these loci are directly occupied by Runx1. We next compared the predicted Runx1 binding sites to DEGs from Runx1-deficient microglia and identified 79 DEGs harboring Runx1 ChIP-seq peaks (Figure 4D; Table S1). Of these, 18 were annotated by IPA as participating in one or more of the pathways shown in Figure 3H, indicating that they are putative direct Runx1 targets involved in inflammatory signaling and other critical microglial functions (Figure 4E).

Microglial Runx1 deficiency reduces opioid antinociception and increases adverse effects

We next asked whether the cellular and transcriptomic changes in microglia impact opioid responses. First, we assessed acute antinociception and found that the response to a single dose of morphine (15 mg/kg i.p.) was attenuated in Runx1-deficient mice that had no prior opioid exposure (Figures 5A and 5B). The requirement for higher doses in morphine-naive mice was consistent with an increase in morphine ED_{50}, indicating diminished antinociceptive potency in both male (Figure 5C) and female (Figure S5A) Runx1-deficient mice. Because opioids are used to manage post-operative pain, we asked whether analgesic requirement is affected in the hind paw incision model of acute post-operative pain. Although mechanical allodynia following hind paw incision was similar in Runx1-deficient and Runx1-expressing mice (Figure 5D), higher doses of morphine were needed to alleviate the post-operative allodynia that developed in Runx1-deficient mice (Figures 5E and 5F). Likewise, a significantly greater amount of morphine was required to attenuate mechanical allodynia in Runx1-deficient mice in the spared nerve injury model of neuropathic pain (Figures S5B and S5C) and following pharmacological disruption of Runx1 by Ro5 in wild-type mice in the complete Freund's adjuvant (CFA) model of inflammatory pain (Figures S5D and S5E). In addition to diminished acute antinociception, Runx1 deficiency exacerbated antinociceptive tolerance (Figures 6A–6C) and morphine-induced hyperalgesia (Figures 6D–6F) following repeated morphine exposure. When mice were rendered morphine dependent, naloxone challenge induced withdrawal behaviors that were more severe in male (Figures 6G–6I) and female (Figure S5F) Runx1-deficient mice as compared with Runx1-expressing mice. Therefore, deletion of Runx1 from microglia blunts morphine antinociception and exacerbates withdrawal behaviors.

(H) Schematic of paradigm used to examine effects of spinal Ro5 treatment on acute response to morphine (15 mg/kg).

(I) Acute antinociceptive response to morphine or SA (CTR), measured using tail-flick latency (TFL) from a thermal stimulus, in male rats treated with Ro5 or CTR. Repeated-measures two-way ANOVA (interaction: $F_{15,160} = 20.4$, $p \leq 0.0001$; time: $F_{5,160} = 62.6$, $p \leq 0.0001$; treatment: $F_{3,32} = 36.11$, $p \leq 0.0001$), Tukey's post hoc test. *As compared with CTR/CTR or Ro5/CTR at each time point post-injection. #Ro5/MS as compared with CTR/MS at each time point post-injection (CTR/MS vs. Ro5/MS: 30 min $p = 0.0010$; 45 min $p < 0.0001$; 60 min $p = 0.0027$; 90 min $p = 0.1190$).

(J) Morphine dose-response median effective dose (ED_{50}) of thermal TFL in male rats treated with Ro5 or CTR. ED_{50} was calculated using non-linear regression fit of dose-response curves in PRISM. CTR 5.7 ± 0.8 mg/kg; Ro5 9.4 ± 1.1 mg/kg. Unpaired two-tailed *t* test ($p = 0.0171$, t = 2.7, df = 13, $p = 0.0171$). Graphs depict mean ± SEM. ****$p < 0.0001$, ***$p < 0.001$, **$p < 0.01$, *$p < 0.05$.

See also Figures S1 and S2.

Please cite this article in press as: Leduc-Pessah et al., Runx1 transcription factor modulates opioid analgesia and withdrawal in humans and rodents, Neuron (2025), https://doi.org/10.1016/j.neuron.2025.11.018

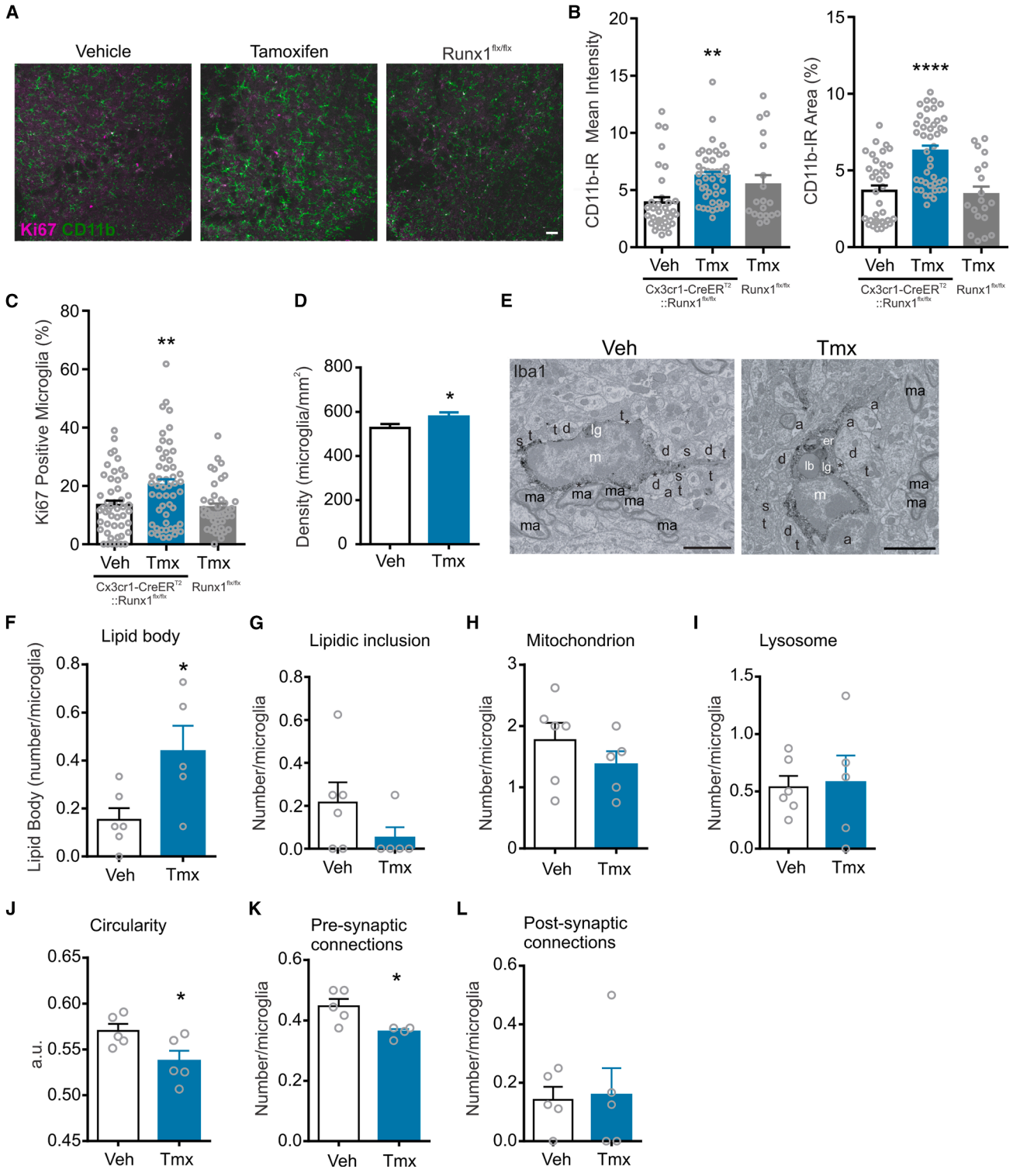

Figure 2. Microglial reactivity is altered in microglia-specific Runx1-deficient mice

(A) Representative immunofluorescent co-labeling of Ki67 with CD11b in lumbar spinal dorsal horn (L4-L5) sections from mice 28 days after treatment with vehicle (Veh) or tamoxifen (Tmx) (images acquired at 20×, scale bar: 50 μm).

(B) Mean intensity of CD11b immunoreactivity (IR) and percent of total area in spinal dorsal horn sections from Veh- and Tmx-treated *Cx3cr1*-Cre^{ERT2}::*Runx1*$^{flx/flx}$ mice and Tmx-treated *Runx1*$^{flx/flx}$ mice (n = 35/43/19 sections from 6/6/3 animals, respectively). One-way ANOVA (intensity: $F_{2,94}$ = 6.76; area: $F_{2,94}$ = 18.09), Sidak's post hoc test.

(legend continued on next page)

Please cite this article in press as: Leduc-Pessah et al., Runx1 transcription factor modulates opioid analgesia and withdrawal in humans and rodents, Neuron (2025), https://doi.org/10.1016/j.neuron.2025.11.018

Since morphine is a potent μ-opioid receptor agonist, it is possible that deletion of Runx1 in microglia affects μ-opioid receptor expression and thereby changes morphine response. On the contrary, both *Oprm1* mRNA transcript and μ-opioid receptor protein expression were comparable in the spinal lumbar cord of Runx1-expressing and Runx1-deficient mice (Figures S6A and S6B). Although *Oprm1* transcripts were not detectable by scRNA-seq analysis, RNAscope fluorescent *in situ* hybridization showed colocalization of *Oprm1* mRNA in Iba1-positive cells in both genotypes (Figure S6C). Furthermore, spinal isolation of microglia-specific transcripts from RiboTag mice (*Cx3cr1*-Cre^{ERT2}::*Rpl22*^{HA}) confirmed the presence of *Oprm1* transcripts in microglia (Figure S6D).[17,22,41,42]

Having established that conditional ablation of Runx1 shifts spinal microglia toward a reactive phenotype and blunts morphine antinociceptive effects, we performed whole-cell patch-clamp recordings in spinal slices to directly measure the effect of morphine on membrane currents in dorsal horn neurons and spontaneous excitatory postsynaptic currents (sEPSCs). We recorded from spinal laminae I-II neurons, a central site for opioid analgesia, confirming that application of morphine evoked an outward current and decreased the amplitude of sEPSCs in Runx1-expressing mice (Figures S7A–S7D). These responses were not detected in Runx1-deficient mice (Figures S7A–S7C and S7E), indicating a diminished morphine-induced postsynaptic effect. Morphine also increased the inter-event interval of sEPSCs in both genotypes (Figures S7F and S7G), but the effect was less pronounced in Runx1-deficient mice (Figures S7F and S7G). sEPSC frequency reflects release from both intrinsic dorsal horn neurons and primary afferent terminals, as well as from descending axon terminals. Since primary afferent excitability remains unaffected in Runx1-deficient mice, the observed partial inhibition of presynaptic morphine action points to a reduced morphine effect on dorsal horn neurons, in agreement with the diminished postsynaptic morphine responses (Figures S7A, S7B, S7D, and S7E). Thus, Runx1 deletion impairs morphine inhibition of spinal dorsal horn circuits, consistent with the partial reduction in morphine antinociceptive potency observed in behavioral experiments.

Runx1 contributes to the differentiation of isolectin B4 (IB4)+ non-peptidergic afferents within the dorsal root ganglia (DRGs), which contain the cell bodies of presynaptic afferents terminating in the spinal dorsal horn.[43–46] We determined that Runx1 protein expression is comparable in DRG isolated from Runx1-expressing and microglia Runx1-deficient mice (Figure S8A), indicating that tamoxifen-induced recombination in *Cx3cr1*-Cre^{ERT2}::*Runx1*$^{flx/flx}$ mice did not impact DRG Runx1 expression. To assess the functional properties of small non-peptidergic neurons, we used whole-cell current clamp to record specifically from biotin-labeled IB4+ small-diameter (<30 pF) DRG neurons (Figures S8B–S8H). In these neurons, capacitance (Figure S8B), resting membrane potential (Figure S8D), rheobase (Figure S8E), action potential half-width (Figure S8F), frequency (Figure S8E), and amplitude (Figure S8H) were comparable in microglial Runx1-expressing and Runx1-deficient mice. Thus, targeted deletion of Runx1 from CX_3CR_1-expressing cells in adult mice does not alter Runx1 expression or excitability of IB4+ sensory neurons.

RUNX1 is a genetic determinant of opioid analgesic requirement and opioid withdrawal severity in humans

Because our findings in rodents demonstrate that Runx1 gates microglia reactivity and opioid responses, we asked whether RUNX1 also modulates human microglia, which express *OPRM1* mRNA transcripts encoding the μ-opioid receptor (Figure 7A).[41,47,48] In human-derived primary microglia culture, we confirmed the presence of RUNX1 and that repeated morphine treatment decreased *RUNX1* transcript levels (Figures 7B and 7C). We also confirmed the localization of RUNX1 in microglia derived from human induced pluripotent stem cell (iPSC) lines (Figure 7D). Application of Ro5 to primary human microglial cultures increased transcript levels of the proinflammatory cytokines IL-1β and IL-6 but reduced the anti-inflammatory cytokine IL-10 (Figure 7E). Ro5 treatment also upregulated TMEM119 and Sall1 without affecting CD68, CD86, or TNF transcripts (Figure 7E). Therefore, RUNX1 exerts important transcriptional control of human microglial reactivity.

Analgesic response to opioid medications and susceptibility to adverse opioid effects are highly variable between individuals.[6] These inter-individual differences hinder effective pain management and increase opioid liability. Given genetic factors may account for 60% of the variability in opioid analgesic response,[49] we examined genetic associations between *RUNX1* variants

(C) Percent of CD11b-positive microglia expressing Ki67 in spinal dorsal horn sections from Veh- and Tmx-treated *Cx3cr1*-Cre^{ERT2}::*Runx1*$^{flx/flx}$ mice and Tmx-treated *Runx1*$^{flx/flx}$ mice (n = 48/51/41 sections from 6/6/3 animals, respectively). One-way ANOVA ($F_{2,137}$ = 6.8), Sidak's post hoc test.
(D) Density of Iba1-positive microglia in the spinal dorsal horn (n = 95/96 images acquired from 6 animals per group). Unpaired two-tailed t test (t = 1.974, df = 189, p = 0.0498).
(E) Representative transmission electron microscopy images within the spinal dorsal horn of Veh- and Tmx-treated *Cx3cr1*-Cre^{ERT2}::*Runx1*$^{flx/flx}$ mice. Images highlight the difference in microglial morphology and identify inclusions within the cells and surrounding elements. Scale bar: 2 μm. Legend: a, astrocyte; d, dendrite; er, endoplasmic reticulum; lb, lipid body; lg, lipofuscin granule; m, microglia; ma, myelinated axon; s, dendritic spine; t, axon terminal; *, microglia-associated extracellular space pockets.
(F) Number of lipid bodies engulfed by Iba1-positive microglia per cell in Veh- and Tmx-treated *Cx3cr1*-Cre^{ERT2}::*Runx1*$^{flx/flx}$ mice. Numbers were averaged per animal (Veh n = 6; Tmx n = 5). Unpaired two-tailed t test (t = 2.558, df = 9, p = 0.0308).
(G) Lipidic inclusions (such as lipofuscin granules) per microglia. Unpaired two-tailed t test (t = 1.458, df = 9, p = 0.1788).
(H) Mitochondria identified and counted per microglia. Unpaired two-tailed t test (t = 1.094, df = 9, p = 0.3025).
(I) Lysosomes identified and counted per microglia. Unpaired two-tailed t test (t = 0.1726, df = 9, p = 0.8668).
(J) Circularity of microglia, with a value of 1.0 indicating a perfect circle and a value approaching 0 indicating an increasingly elongated shape. Unpaired two-tailed t test (t = 2.408, df = 8, p = 0.0426).
(K and L) Number of direct microglial contacts with (K) presynaptic elements (unpaired two-tailed t test, t = 2.969, df = 7, p = 0.0208) and (L) postsynaptic elements (unpaired two-tailed t test, t = 0.1636, df = 8, p = 0.8741). Graphs depict mean ± SEM. ****p < 0.0001, **p < 0.01, *p < 0.05.
See also Figure S3.

Please cite this article in press as: Leduc-Pessah et al., Runx1 transcription factor modulates opioid analgesia and withdrawal in humans and rodents, Neuron (2025), https://doi.org/10.1016/j.neuron.2025.11.018

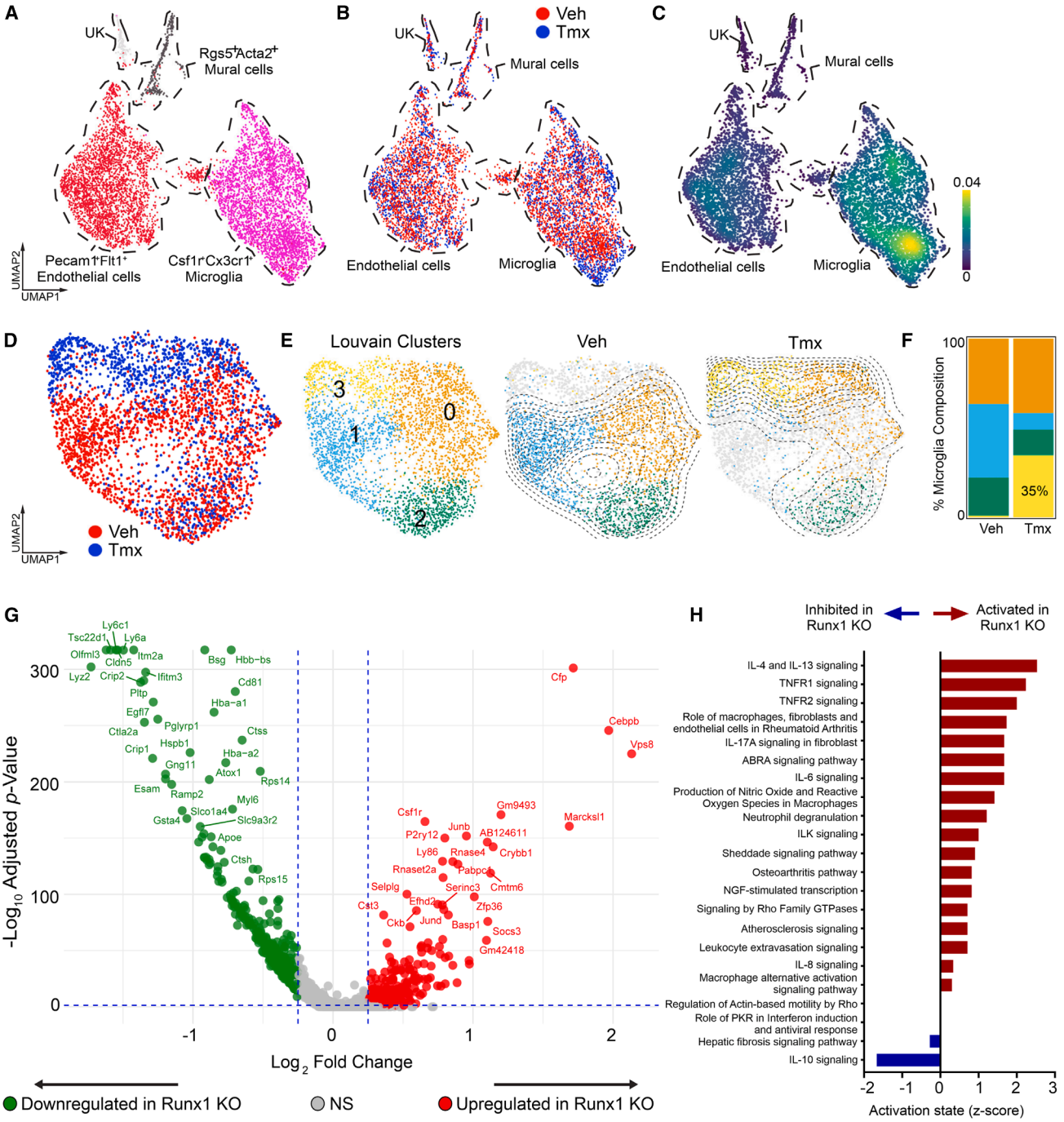

Figure 3. Single-cell transcriptomics reveals alterations in microglial states in Runx1-deficient mice

(A and B) Uniform manifold approximation and projection (UMAP) of all recovered cells from vehicle (Veh) and tamoxifen (Tmx)-treated *Cx3cr1*-Cre^{ERT2}::*Runx1*$^{flx/flx}$ mice, identified by cell type (A) and sample IDs (B).

(C) Kernel density estimate depicting magnitude of transcriptional deviation across Veh- and Tmx-treated mice for each cell type.

(D and E) Subclustered microglia states, colored by (D) sample IDs and (E) Louvain cluster distribution across Veh- and Tmx-treated mice.

(F) Stacked bar depicting microglia subcluster composition.

(G) Volcano plot depicting microglial DEGs in Runx1-knockout(Runx1-KO, Tmx-treated) compared with Veh-treated *Cx3cr1*-Cre^{ERT2}::*Runx1*$^{flx/flx}$ mice (cutoff value: ±0.25 $\log_2$ fold change, $p_{adj} < 0.05$).

(H) Predicted activation states for the top pathways (defined by *p* value) identified by IPA. Of the top 25 pathways ($p < 0.001$ for all, Benjamini-Hochberg correction), activation states were not available for the following: agranulocyte adhesion and diapedesis, granulocyte adhesion and diapedesis, and hepatic fibrosis/hepatic stellate cell activation. The complete list of pathways is presented in Table S1.

See also Figure S4.

Please cite this article in press as: Leduc-Pessah et al., Runx1 transcription factor modulates opioid analgesia and withdrawal in humans and rodents, Neuron (2025), https://doi.org/10.1016/j.neuron.2025.11.018

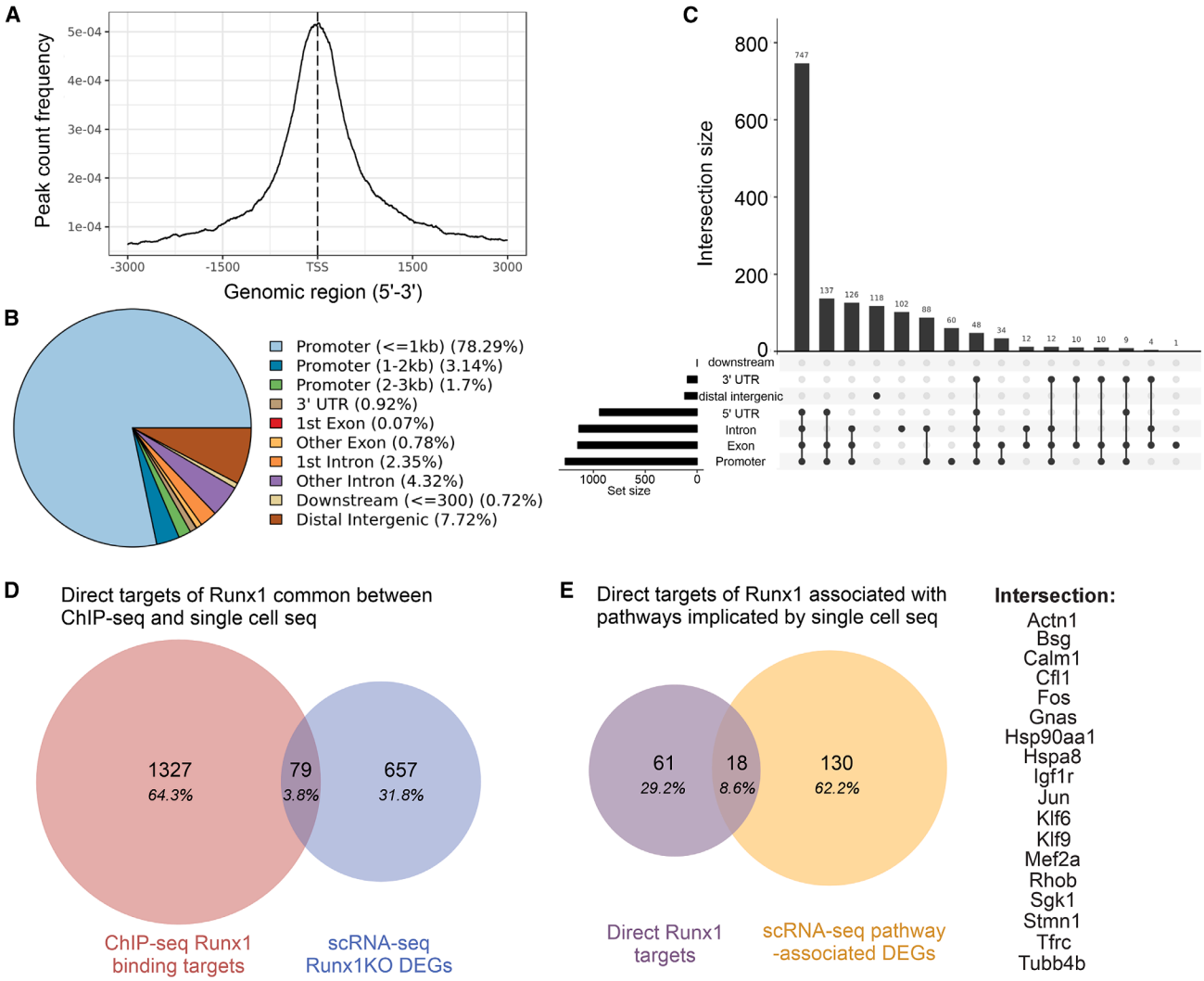

Figure 4. Genome-wide identification of Runx1 binding sites in spinal cord cells by ChIP sequencing

(A) Average profile of ChIP-seq peaks falling within ±3 kb of annotated transcription start site (TSS) regions.

(B) Composition of peaks annotated based on the genomic features they overlap. When annotations overlapped, assignment priorities were promoter > 5′ UTR > 3′ UTR > exon > intron > downstream > intergenic.

(C) Histogram of features overlapped by peaks, ranked by number of peaks.

(D) Diagram depicting overlap between predicted Runx1 binding targets (identified by ChIP-seq in ≥2 of 3 biological replicates) and DEGs identified in Runx1-deficient microglia by single-cell sequencing (Figure 3G).

(E) Diagram depicting overlap between direct Runx1 transcriptional targets (Runx1 binding targets ∩ Runx1 knockout [KO] DEGs) identified in (D) and Runx1 KO DEGs associated with one or more of the 25 pathways described in Figure 3H.

See also Figure S4.

and differences in opioid requirement in two independent human post-operative pain cohorts. First, we extracted specific data for the human *RUNX1* gene region from a previously performed genome-wide association study (GWAS) in patients that underwent cosmetic orthognathic surgery for mandibular prognathism (n = 355).[50] Linkage disequilibrium (LD) analysis for this region identified 21 Tag single-nucleotide polymorphisms (SNPs). Association analysis of these SNPs revealed that SNP rs2236431, situated within the *RUNX1* transcription factor binding site (Figure 8A), was significantly associated with total perioperative analgesic use (Figures 8B and S9A; Table S2). Specifically, the major allele homozygotes (A/A) for this intronic *RUNX1* SNP required more peri-operative analgesics than heterozygotes (A/C) and minor allele homozygotes (C/C) (Figures 8B and S9A). While several other neighboring SNPs were in high LD (r^2 > 0.6) with rs2236431, they did not exhibit stronger associations with opioid analgesia-related phenotypes in this cohort (Figure S10; Table S2). However, rs2236431 was not associated with 24 h post-operative pain scores, indicating that the *RUNX1* polymorphism did not impact acute pain severity following surgery (Table S2). In a validation cohort of patients who underwent major abdominal surgery (n = 112),[51] rs2236431 was also

Please cite this article in press as: Leduc-Pessah et al., Runx1 transcription factor modulates opioid analgesia and withdrawal in humans and rodents, Neuron (2025), https://doi.org/10.1016/j.neuron.2025.11.018

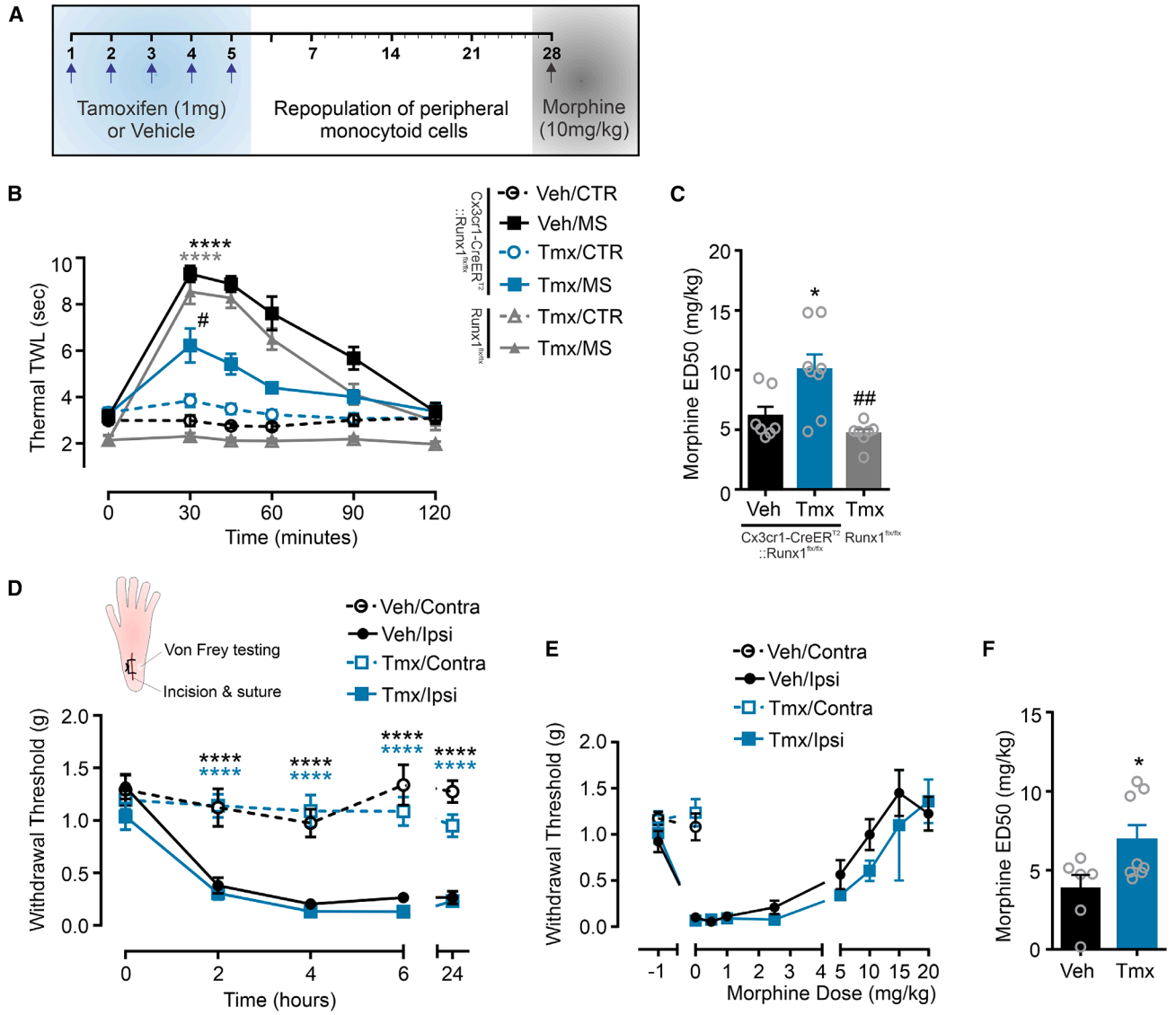

Figure 5. Antinociceptive response to morphine is reduced in Runx1-deficient mice, and the requirement for opioids is increased in a model of post-surgical pain

(A) Schematic of drug administration paradigm used to induce microglial knockout of Runx1 and allow repopulation of peripheral CX_3CR_1-positive cells.

(B) Antinociceptive response to acute morphine sulfate (MS; 10 mg/kg) in vehicle (Veh) or tamoxifen (Tmx) treated male mice on post-Veh/Tmx day 28, measured using tail withdrawal latency (TWL) from a 50°C water bath. Repeated-measures two-way ANOVA (interaction $F_{18,132} = 29.4$, $p \leq 0.0001$; time $F_{4,132} = 128$, $p \leq 0.0001$; treatment $F_{5,37} = 43.0$, $p \leq 0.0001$), Tukey's post hoc test. Veh-treated: $n = 8$; Tmx-treated: $n = 7$ mice per group. ****$p < 0.0001$, as compared with the respective SA-treated group (CTR) at 30 min post-injection. ####$p < 0.0001$ Tmx/MS vs. Veh/MS.

(C) Morphine dose-response median effective dose (ED_{50}) of thermal TWL as measured in Veh- and Tmx-treated mice. ED_{50} was calculated using non-linear regression fit of dose-response curves in PRISM. Veh 6.1 ± 0.8 mg/kg; Tmx 10.0 ± 1.3 mg/kg; *Runx1*$^{flx/flx}$ 4.7 ± 0.4 mg/kg. One-way ANOVA (Veh, $n = 7$; Tmx, $n = 8$; *Runx1*$^{flx/flx}$, $n = 7$) ($F_{2,19} = 9.01$), Sidak's post hoc test. *$p < 0.05$ compared with Veh ($p = 0.0163$). ##$p < 0.01$ compared with Tmx ($p = 0.0013$).

(D) Mechanical paw withdrawal thresholds measured before and 2, 4, 6, and 24 h after incision in the plantar surface of the hind paw. Ipsilateral and contralateral thresholds were compared at each time point. Two-way repeated-measures ANOVA (interaction $F_{12,128} = 6.4$; time $F_{4,128} = 28.6$; treatment $F_{3,32} = 33.3$; subjects $F_{32,128} = 3.2$), Tukey's post hoc test ($n = 8$, 10). ****$p < 0.0001$.

(E) Morphine dose-response at 4 h post-incision in Veh- and Tmx-treated mice.

(F) ED_{50} of mechanical thresholds. Veh ($n = 6$) 3.8 ± 0.9 mg/kg; Tmx ($n = 8$) 6.9 ± 1.0 mg/kg. Unpaired two-tailed *t* test (t = 2.3, df = 12, $p = 0.0414$). *$p < 0.05$ compared with Veh. Graphs depict mean ± SEM.

See also Figures S3 and S5.

Please cite this article in press as: Leduc-Pessah et al., Runx1 transcription factor modulates opioid analgesia and withdrawal in humans and rodents, Neuron (2025), https://doi.org/10.1016/j.neuron.2025.11.018

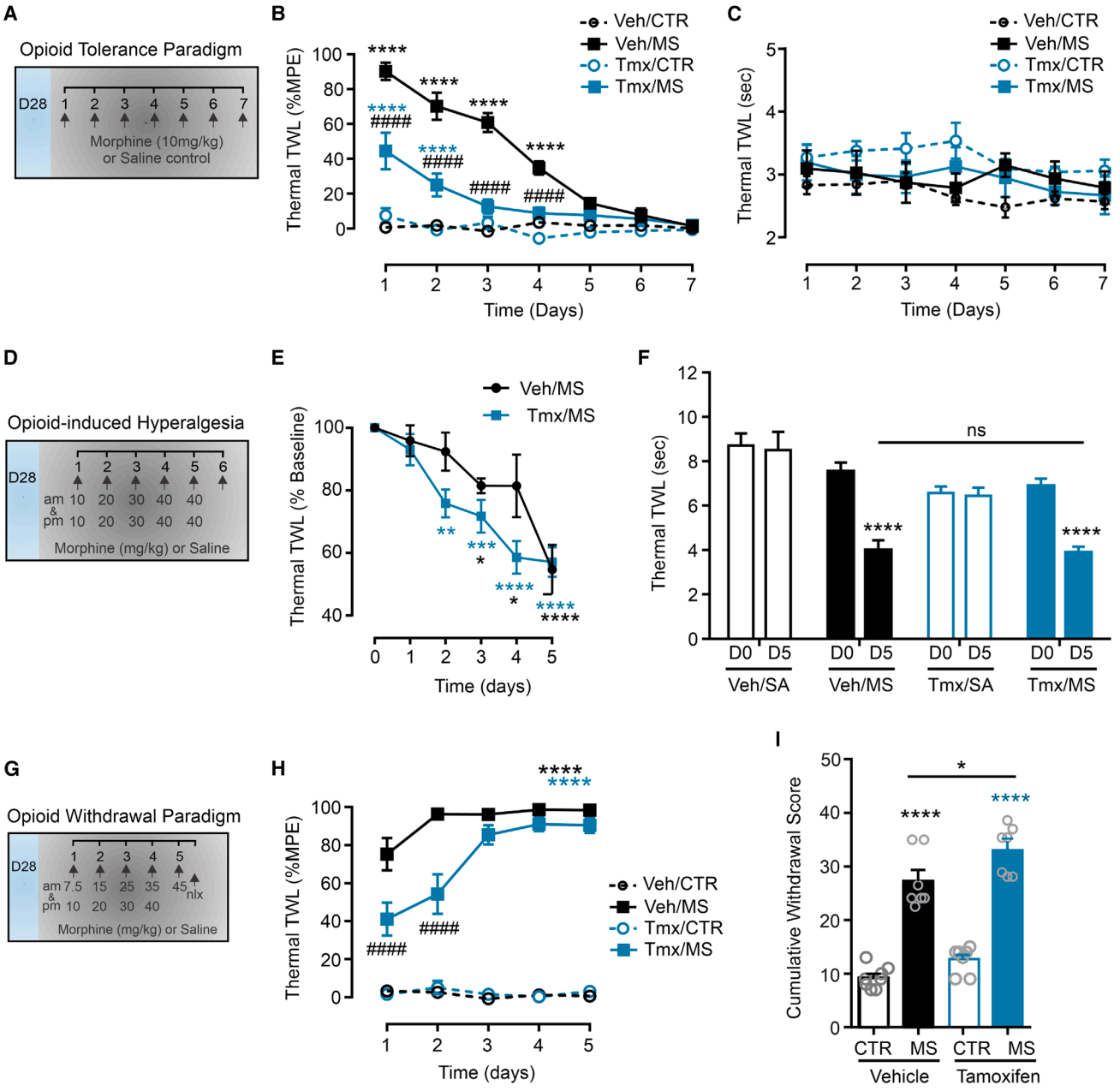

Figure 6. Accelerated development of morphine analgesic tolerance and opioid-induced hyperalgesia in Runx1-deficient mice

(A) Morphine dosing paradigm used to induce antinociceptive tolerance. Starting at day 28 post first tamoxifen (Tmx) or vehicle (Veh) injection, mice were treated with morphine sulfate (MS, 10 mg/kg) or SA (CTR) once daily.

(B) Daily antinociceptive response to morphine measured using tail withdrawal latency (TWL) from a 50°C water bath before and 30 min after injection. TWL is reported as a percentage of the maximum possible effect (%MPE). Repeated-measures two-way ANOVA (interaction $F_{18,144} = 17.3$; time $F_{6,144} = 43.4$; treatment $F_{3,24} = 143$; subjects $F_{24,144} = 1.1$), Dunnett's post hoc test ($n = 7$). ****$p < 0.0001$, as compared with the respective CTR-treated group on each day of treatment. ####$p < 0.0001$ Tmx/MS as compared with Veh/MS treatment groups.

(C) Daily baseline TWL from a 50°C water bath.

(D) Paradigm for opioid-induced hyperalgesia. Starting at day 28 post first tamoxifen injection, mice were treated with escalating doses of morphine or SA twice daily, at 10-h intervals, for 5 days.

(E) Daily thermal nociceptive thresholds in Veh and Tmx morphine-treated mice, measured before a.m. morphine injection, using TWL from a 48°C water bath. TWL is reported as a percentage of the baseline latency. Repeated-measures two-way ANOVA (interaction $F_{5,65} = 2.3$; time $F_{5,65} = 25.1$; treatment $F_{1,13} = 3.2$; subjects $F_{13,65} = 3.1$), Dunnett's post hoc test ($n = 7, 8$). Daily thresholds were compared with their own baseline values on day 0. ****$p < 0.0001$, **$p < 0.01$, *$p < 0.05$.

(legend continued on next page)

Please cite this article in press as: Leduc-Pessah et al., Runx1 transcription factor modulates opioid analgesia and withdrawal in humans and rodents, Neuron (2025), https://doi.org/10.1016/j.neuron.2025.11.018

associated with total post-operative rescue analgesic dose (Figures 8C and S9B). We found that homozygous A/A individuals required higher doses of rescue analgesic medication than heterozygous A/C and minor allele homozygous (C/C) individuals (Figure 8C). Although only three individuals in this study were homozygous for the minor C allele, none required rescue analgesic medication after abdominal surgery (Figure S9B). In both the mandibular and abdominal post-operative pain cohorts, rs2236431 remained significantly associated with opioid analgesic response and dependence after adjusting for SNPs in the *OPRM1* gene (rs1799971) encoding the μ-opioid receptor, the *ABCB1* gene (rs1045642) responsible for the ATP-Binding Cassette B1 Transporter, and the *CREB1* gene (rs2952768) that encodes the cAMP-responsive element-binding protein 1 (CREB1) transcription factor. Therefore, *RUNX1* rs2236431 is unique and independent from these SNPs, which have known associations with opioid analgesic response or dependence.[52,53]

Finally, we examined the association between *RUNX1* SNPs and opioid withdrawal severity, the sum of fifteen assessed withdrawal symptoms, reported by 1,226 opioid-dependent individuals in the Comorbidity and Trauma Study (CATS).[54,55] Linear regression analyses with opioid withdrawal symptom count as the dependent variable[54,55] identified 18 nominally significant *RUNX1* SNPs (rs2236431 did not reach this threshold). After a correction for multiple testing, a single association signal consisting of three SNPs in high LD remained significant (e.g., rs75792166 adjusted *p* value 7.50E−03) (Figure S9C). Thus, multiple *RUNX1* polymorphisms significantly contribute to variability in clinically relevant opioid phenotypes: peri- and post-operative opioid analgesic requirements and opioid withdrawal severity.

DISCUSSION

In this study, we uncovered that repeated morphine exposure disrupts Runx1 transcriptional inhibition of microglia. Runx1 is a transcriptional repressor critical for microglia quiescence and differentiation: it is a "molecular brake" that suppresses microglial reactivity.[32,56–58] Morphine "releases" this brake, which is unexpected and ascribes a functional importance of Runx1 in the adult central nervous system with mechanistic and potential therapeutic relevance in modulating opioid analgesic responses and adverse outcomes. In rodents, disrupting Runx1 transcriptional activity caused aberrant microglial reactivity and diminished opioid analgesic potency, while worsening opioid withdrawal and hyperalgesia. Inhibition of Runx1 also diminished morphine antinociception following peripheral nerve injury or CFA-induced inflammation, an effect that may reflect reduced morphine potency or an exacerbated pain phenotype. Furthermore, we demonstrate that genetic targeting of Runx1 induces ultrastructural changes and the emergence of a transcriptomic signature consistent with a reactive microglial phenotype. That not all spinal microglia displayed this transcriptomic change is consistent with the spatiotemporal heterogeneity of microglia reported in mice and humans.[59–61] The shift in spinal microglia subpopulations coincides with weakened, but not abolished, morphine inhibition of pain-signaling neurons in spinal laminae I–II. This change may account for the reduced morphine antinociceptive responses observed in microglia from Runx1-deficient mice.

To determine the impact of microglial Runx1 deficiency on opioid modulation of excitatory synaptic transmission in the spinal dorsal horn, we measured holding currents and sEPSCs. Although dorsal-root-evoked recordings can offer insight into primary afferent terminals, we focused on spontaneous events for several reasons. First, sEPSCs provide information on the integrated influence of both intrinsic dorsal horn neurons and extrinsic afferent inputs, allowing assessment of the overall morphine effect on dorsal horn neuron excitatory drive. By contrast, afferent-evoked responses only provide a partial measure of morphine action. Second, our approach allowed us to evaluate both the pre- and postsynaptic effects of morphine. In particular, we confirmed that morphine induced an outward current and reduced sEPSC amplitude, effects that were rendered undetectable by Runx1 deletion. Morphine also decreased sEPSC frequency, but this action was significantly attenuated rather than eliminated in Runx1-deficient mice. The persistence of changes in the frequency of sEPSCs, accompanied by unaltered postsynaptic currents, suggests that microglial Runx1 deletion selectively blunts morphine's postsynaptic modulation, with relatively limited presynaptic effects. Third, the technical stability of sEPSC recordings is greater than evoked EPSCs, which can vary substantially with minor differences in stimulus intensity, root preservation, and electrode positioning, complicating quantitative comparisons. Together, these factors make sEPSCs a robust, physiologically relevant readout for detecting Runx1-dependent changes in opioid modulation. Nonetheless, evoked EPSC studies could complement these findings and represent a valuable direction for future work.

Runx1 regulates peripheral nociceptor specification and differentiation during development, as well as the expression of

(F) Day 0 (baseline) and day 5 TWL in mice treated with morphine or SA. SA-treated mice showed no change in thermal thresholds, whereas morphine-treated mice showed a significant reduction. The Veh/MS and Tmx/MS groups are the same data reported in (E). Repeated-measures two-way ANOVA (interaction $F_{3,26} = 12.9$; time $F_{1,26} = 47.1$; treatment $F_{3,26} = 14.2$; subjects $F_{26,26} = 2.3$) Sidak's post hoc test ($n = 7, 7, 8, 8$). ****$p < 0.0001$ as compared with day 0.
(G) Paradigm for opioid physical dependence and withdrawal. Starting at day 28 post first tamoxifen injection, mice were treated with escalating doses of morphine or SA twice daily, at 8-h intervals, for 5 days. Naloxone-precipitated withdrawal was induced 2 h after the final morphine injection (day 5 a.m.), and withdrawal behaviors were scored for 30 min.
(H) Daily antinociceptive response to a.m. morphine injection in Veh- and Tmx-treated mice. Morphine antinociception was measured using TWL from a 50°C water bath before and 30 min after injection. TWL is reported as %MPE. Repeated-measures two-way ANOVA ($n = 7$) (interaction $F_{12,96} = 7.6$; time $F_{4,96} = 12.4$; treatment $F_{3,24} = 531.1$; subjects $F_{24,96} = 1.2$), Tukey's post hoc test.
(I) Cumulative withdrawal score following naloxone-precipitated withdrawal in Veh- and Tmx-treated female mice treated with SA or morphine for 5 days ($n = 4, 5$). Unpaired two-tailed *t* test ($t = 2.980$, $df = 7$, $p = 0.0205$). ****$p < 0.0001$, as compared with the respective CTR-treated group each day. ####$p < 0.0001$ Tmx/MS as compared with the Veh/MS treatment group each day. Graphs depict mean ± SEM.
See also Figures S3 and S5.

Please cite this article in press as: Leduc-Pessah et al., Runx1 transcription factor modulates opioid analgesia and withdrawal in humans and rodents, Neuron (2025), https://doi.org/10.1016/j.neuron.2025.11.018

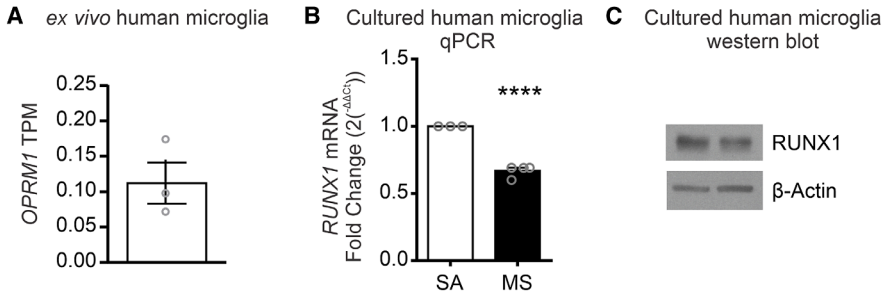

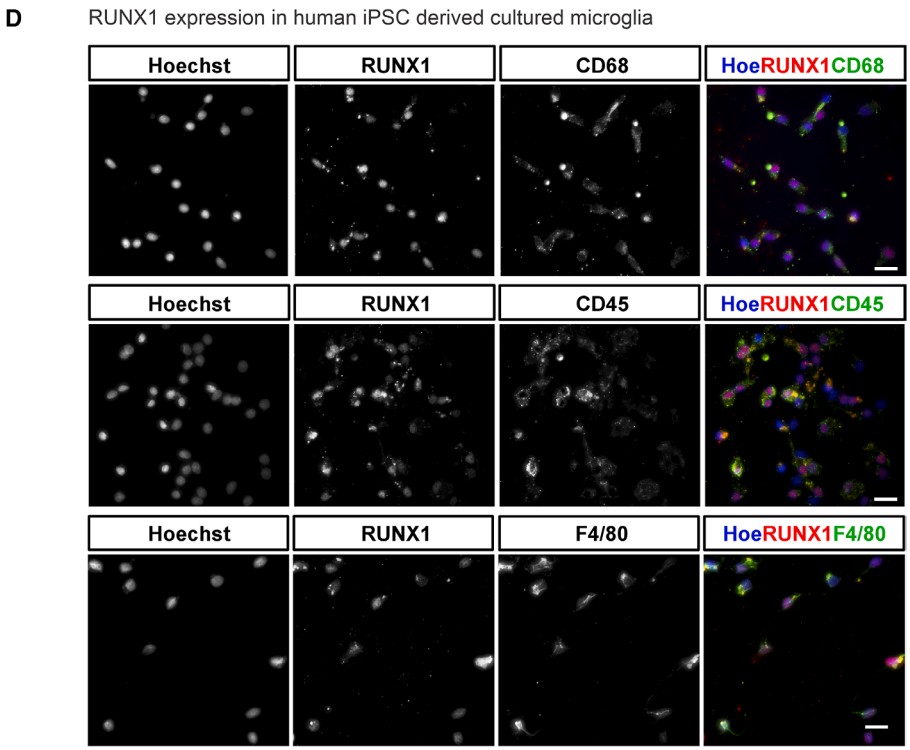

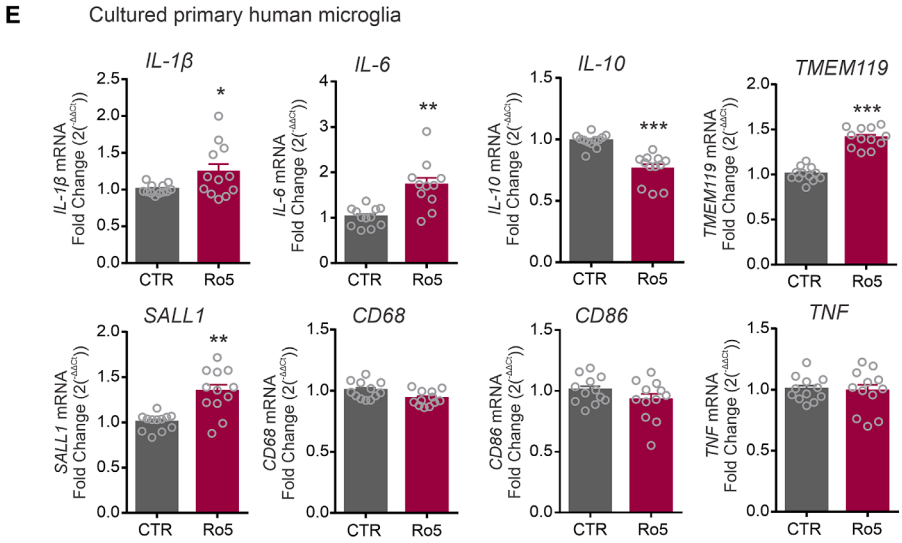

(legend on next page)

Please cite this article in press as: Leduc-Pessah et al., Runx1 transcription factor modulates opioid analgesia and withdrawal in humans and rodents, Neuron (2025), https://doi.org/10.1016/j.neuron.2025.11.018

genes involved in nociceptor function.[43,44,62] In contrast to its central effects, our findings indicate that cell-specific ablation of Runx1 does not alter peripheral nociceptive processing. Notably, *Cx3cr1*-Cre^{ERT2}::*Runx1*$^{flx/flx}$ mice, which express microglial Runx1 from development through adulthood until tamoxifen-induced deletion, displayed normal nociceptive thresholds, maintained DRG Runx1 expression, and exhibited intact activity of small-diameter IB4+ sensory DRG neurons. These results suggest that the opioid phenotype observed in microglial Runx1-deficient mice is unlikely to arise from changes in peripheral nociceptive function. Nevertheless, we acknowledge that intrathecal administration of Ro5 in adult rodents could exert both central and peripheral effects, and we cannot exclude a contribution of DRG-mediated mechanisms in this experimental context.

In humans, we identified significant associations between *RUNX1* polymorphisms and both greater post-operative opioid analgesic requirements and more severe opioid withdrawal symptoms. Although these associations cannot be specifically attributed to Runx1 function in microglia, which is a key limitation of the study, our data confirm that human microglia express RUNX1 and that pharmacological RUNX1 inhibition shifts microglia toward a proinflammatory and reactive profile similar to that observed in rodents. While *RUNX1* has not been implicated in opioid-related traits in large-scale GWAS or phenome-wide association study (PheWAS) analyses, this does not preclude the relevance of our findings. Notably, our study employed a conditional, microglia-specific Runx1 knockout model, resulting in targeted gene ablation in a defined cellular context. By contrast, GWASs detect associations with common variants that typically have subtle, context-dependent effects. Moreover, few large GWASs have focused specifically on opioid responses, meaning such effects may not be represented under the baseline or population-wide conditions typically captured in GWAS or PheWAS datasets. Opioid-related phenotypes—such as perioperative requirements, withdrawal severity, or addiction susceptibility—are complex, influenced by environmental factors, and often not well represented in large population databases (e.g., UK Biobank). These phenotypes are best studied under defined clinical or experimental conditions. Therefore, the absence of a GWAS signal for *RUNX1* likely reflects limitations in trait representation, tissue specificity, and statistical power, rather than a lack of biological relevance.

Our analyses further reveal that *RUNX1* rs2236431 is significantly associated with opioid analgesic responses in two independent human post-operative pain cohorts. Although rs2236431 is an intronic variant, functional annotation indicates that rs2236431 is located within a distal enhancer-like candidate *cis*-regulatory element in the *RUNX1* locus and is adjacent to multiple transcription factor binding motifs, based on UCSC Genome Browser and ENCODE data (https://genome.ucsc.edu/). Although the precise regulatory consequences remain to be experimentally validated, this genomic context supports a model in which rs2236431 modulates *RUNX1* transcriptional activity or autoregulation, thereby influencing microglial function. Our rodent studies provide orthogonal functional support, demonstrating that microglia-specific Runx1 deletion alters transcriptomic profiles and chromatin occupancy consistent with a reactive microglial phenotype. However, it remains unclear whether rs2236431 directly affects *RUNX1* expression or microglial function. While our *in vitro* experiments show that pharmacologically inhibiting RUNX1 alters human microglial responses, we cannot attribute these effects to this specific SNP. Future studies incorporating expression quantitative trait loci (eQTL) analyses and allele-specific functional assays in human microglia will be necessary to address this question.

Recent cross-species and multi-omic studies further support the relevance of *RUNX1* to pain and opioid-related phenotypes. Chen et al.[63] used integrative human PheWAS and mouse pain models to identify gene modules associated with neuropathic pain. *RUNX1* was upregulated in pain models and emerged as a hub gene within pain-related transcriptional networks. Similarly, Phan et al.[64] used scRNA-seq and SCENIC network analysis to identify RUNX1 as a microglia-enriched transcription factor in the human dorsal striatum, a region implicated in opioid use disorder. Epigenetic studies further implicate *RUNX1* in opioid-related neurobiology: Tang et al.[65] reported that RUNX1 modulates GAD2 gene methylation in the context of opioid use disorder, while Radhakrishna et al.[66] observed altered *RUNX1* methylation within cytokine-related pathways in placental tissue from opioid-exposed pregnancies, suggesting contributions to neonatal opioid withdrawal syndrome and neuroimmune signaling. Collectively, these studies highlight a broader, context-dependent role for RUNX1 in neuroimmune modulation, pain regulation, and opioid response.

In summary, our data from rats, mice, and human microglia provide cross-species evidence that Runx1 modulates microglial responses. Further, our findings suggest that individuals carrying functional variants such as rs2236431 may be at increased risk for reduced opioid efficacy or heightened adverse effects. While no approved therapies currently exist to directly modulate RUNX1 activity, future strategies could include pharmacogenomic screening to identify individuals less likely to benefit

Figure 7. Microglial reactivity is altered in response to Runx1 inhibition in human cultured spinal microglia

(A) Microglia bead-selected from human brain tissue were sequenced and assessed for *OPRM1* expression (TPM, transcript per million).

(B) Primary cultured microglia from human brain tissue were treated with morphine sulfate (MS, 10 μM, $n = 4$) or saline (SA, $n = 3$) for 5 days and collected for qPCR analysis. *RUNX1* mRNA is expressed relative to the SA group. Unpaired *t* test (t = 12.4, df = 5, $p \leq 0.0001$).

(C) Primary cultured microglia from human brain tissue were pooled and collected for western blot.

(D) Immuno-labeling of microglia derived from human iPSC lines. Runx1 co-immunolabeling with CD68, CD45, and F4/80 (microglial markers). Hoechst (Hoe) stain identifies nuclei (images acquired at 60×; scale bars: 50 μm).

(E) Primary cultured microglia from human brain tissue were treated with Ro5 (0.5 μM) or vehicle control (CTR) for 5 days and collected for PCR analysis ($n = 12$; 3 plates each from 4 independent human samples). mRNA levels are expressed relative to the CTR group. Unpaired *t* tests: IL-1β (t = 2.239, df = 11, $p = 0.0467$), IL-6 (t = 3.770, df = 10, $p = 0.0037$), IL-10 (t = 5.657, df = 11, $p = 0.0001$), TMEM119 (t = 9.290, df = 11, $p \leq 0.0001$), SALL1 (t = 4.595, df = 11, $p = 0.0008$), CD68 (t = 2.149, df = 11, $p = 0.0547$), CD86 (t = 1.518, df = 11, $p = 0.1573$), and TNF (t = 0.218, df = 11, $p = 0.8312$). Graphs depict mean ± SEM. $^{****}p < 0.0001$, $^{***}p < 0.001$, $^{**}p < 0.01$, $^{*}p < 0.05$.

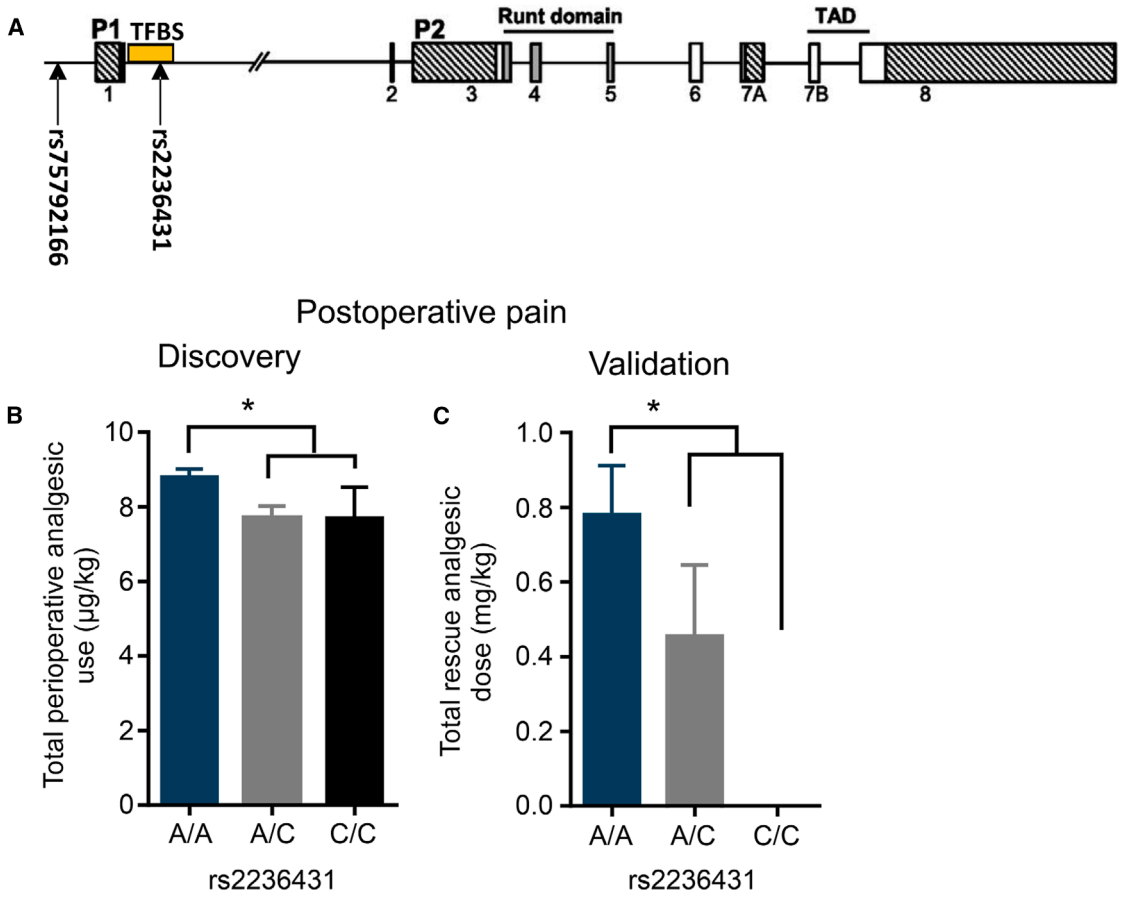

Figure 8. Withdrawal severity is increased in humans with a genetic variant of *RUNX1*

(A) Schematic of the human *RUNX1* gene indicating locations of the identified SNPs in relation to the promoters (P1 and P2) and exons (1–8). According to the UCSC Genome Browser ORegAnno, track transcription factor binding site (TFBS) overlaps with rs2236431; however, the TFBS region is not well characterized and may be cell-type specific.

(B) Association between the total perioperative analgesic use and genotype of the rs2236431 SNP in a cohort of patients who underwent cosmetic orthognathic surgery for mandibular prognathism. Comparisons were made between the dominant A/A genotype ($n = 232$) and the A/C ($n = 103$) + C/C ($n = 17$) genotype groups of the SNP. Further details are outlined in Figure S9A.

(C) Association between the total dose of rescue analgesic administration and genotype of the rs2236431 SNP in major abdominal surgery subjects. Comparisons were made between the AA ($n = 65$) and AC ($n = 21$) genotype groups. Further details are outlined in Figure S9B. CATS association analysis results are shown in Figure S9C. Graphs depict mean ± SEM. *$p < 0.05$.

See also Figure S10 and Table S2.

from opioid analgesics, enabling personalized treatment incorporating alternative analgesics. Although speculative, approaches aimed at restoring or enhancing RUNX1 function—such as small-molecule modulators or gene-based strategies—may offer novel therapeutic avenues. Further studies are needed to elucidate the cellular impact of RUNX1 variants and to assess the feasibility and safety of such interventions. Collectively, our findings underscore the potential for personalized opioid pain management by identifying individuals at risk for poor analgesic response or adverse opioid outcomes.

RESOURCE AVAILABILITY

Lead contact

Requests for further information and resources should be directed to and will be fulfilled by the lead contact, Tuan Trang (trangt@ucalgary.ca).

Materials availability

This study did not generate new, unique reagents.

Data and code availability

All sequencing data have been deposited at the Gene Expression Omnibus (GEO) and can be located under accession number GEO: GSE253853 (token: yxctagwuftaphgx). This paper does not report original code. Any additional information required to reanalyze the data reported in this paper is available from the lead contact upon request.

ACKNOWLEDGMENTS

We thank Rita Lo for assistance in running western blots with human samples, Dr. Nancy Speck's laboratory (UPenn) for providing *Runx1*$^{flx/flx}$ breeding pairs, Drs. Dan Littman (HHMI, NYUSM) and Wen-Biao Gan (NYUSM) for the *Cx3cr1*-Cre^{ERT2} breeding pairs, and the Hotchkiss Brain Institute Advanced Microscopy Platform. This work was supported by grants from the Canadian Institutes of Health Research (CIHR; PJT-173553 and PJ8-169697) and the Natural

Sciences and Engineering Research Council of Canada (RGPIN06289-2019) (T.T.), a CIHR Foundation grant (FDN-159906) and Canada Research Chair in Chronic Pain and Related Brain Disorders (Y.D.K.), an Excellence Scholarship from Wallonie-Bruxelles International (J.D.), a CIHR Foundation grant (PJT-189975) and Calgary Firefighters Burn Treatment Society Chair (J.B.), a CIHR Fellowship (B.B.M.), CIHR Vanier and Killam Doctoral Scholarships (S. Sinha), an ALS Canada Grant (S. Stifani), grants from the Japan Society for the Promotion of Science (JSPS) KAKENHI (20K09259 and 17K08970) (D.N.), and grants from the JSPS (21H03028, 17H04324, 23K21457, and JP22H04922 [AdAMS]) and Japan Agency for Medical Research and Development (JP19ek0610011) (K.I.). Finally, we are grateful for the generous donation from Donna and Rod Evans.

AUTHOR CONTRIBUTIONS

Conceptualization, H.L.-P., T.T., S. Stifani, and J.B.; methodology, H.L.-P., B.B.M., T.T., S. Stifani, J.D., E.M.-P., Y.D.K., F.V., S. Sinha, and J.B.; investigation, H.L.-P., B.B.M., S. Sinha, S.S.-H., D.N., C.Y.F., M.-K.S.-P., A.B., M.D., N.E.B., J.D., E.M.-P., F.V., L.M.H., J.C.-P., N.J.v.d.H., Z.Z., F.T.T.A., V.E.C.P., M.M., K.-i.F., Y.M.T., T.I., M.N., M.H., E.J., A.A., L.D., and N.G.M.; formal analysis, H.L.-P., B.B.M., N.E.B., S. Sinha, D.N., M.-K.S.-P., J.D., E.M.-P., A.B., M.D., L.M.H., K.-i.F., Y.M.T., T.I., M.N., M.H., E.C.N., E.J., A.A., L.D., and N.G.M.; data curation, S. Sinha; writing – original draft, H.L.-P. and T.T.; writing – review & editing, H.L.-P., T.T., B.B.M., C.B., K.I., E.C.N., E.J., A.A., and L.D.; supervision, G.W.Z., E.C.N., C.A., M.-E.T., C.B., S. Stifani, Y.D.K., K.I., J.B., and T.T.; funding acquisition, E.C.N., C.A., M.-E.T., C.B., S. Stifani, Y.D.K., K.I., J.B., and T.T.

DECLARATION OF INTERESTS

T.T. is co-founder and CEO of and holds equity in AphioTx Inc. C.B. is the founder of and holds equity in Sequence2Script Inc. J.B. is co-founder/scientific lead and holds equity in FibroDynamx Inc.

STAR★METHODS

Detailed methods are provided in the online version of this paper and include the following:

- KEY RESOURCES TABLE
- EXPERIMENTAL MODEL AND STUDY PARTICIPANT DETAILS
  - Animals
  - Cell lines
  - Primary cell cultures
  - Human participants
- METHOD DETAILS
  - Rodent surgeries and behavioral testing
  - Protein assessment
  - Electron microscopy
  - RNA assessment
  - Cell isolation for FACS
  - Single-cell transcriptional profiling
  - Chromatin immunoprecipitation sequencing
  - Chromatin immunoprecipitation qPCR
  - Spinal cord electrophysiology recordings
  - DRG electrophysiology recordings
  - Post-operative analgesic use studies
  - Comorbidity and Trauma Study
- QUANTIFICATION AND STATISTICAL ANALYSIS
  - General statistical analysis
  - Spinal cord electrophysiology recordings
  - Human genetic association studies

SUPPLEMENTAL INFORMATION

Supplemental information can be found online at https://doi.org/10.1016/j.neuron.2025.11.018.

Received: April 3, 2025
Revised: October 8, 2025
Accepted: November 17, 2025

REFERENCES

1. Montgomery, L.S. (2022). Pain management with opioids in adults. J. Neurosci. Res. *100*, 10–18. https://doi.org/10.1002/jnr.24695.
2. Kalso, E., Edwards, J.E., Moore, A.R., and McQuay, H.J. (2004). Opioids in chronic non-cancer pain: systematic review of efficacy and safety. Pain *112*, 372–380. https://doi.org/10.1016/j.pain.2004.09.019.
3. Bakare, T.T., Uzoeto, H.O., Gonlepa, L.N., Cosmas, S., Ajima, J.N., Arazu, A.V., Ezechukwu, S.P., Didiugwu, C.M., Ibiang, G.O., Osotuyi, A.G., et al. (2024). Evolution and challenges of opioids in pain management: Understanding mechanisms and exploring strategies for safer analgesics. Med. Chem. Res. *33*, 563–579. https://doi.org/10.1007/s00044-024-03207-1.
4. Solhaug, V., and Molden, E. (2017). Individual variability in clinical effect and tolerability of opioid analgesics - Importance of drug interactions and pharmacogenetics. Scand. J. Pain *17*, 193–200. https://doi.org/10.1016/j.sjpain.2017.09.009.
5. Durgin, C.J., Huhn, A.S., Bergeria, C.L., Finan, P.H., Campbell, C.M., Antoine, D.G., and Dunn, K.E. (2023). Within subject, double blind, examination of opioid sensitivity in participant-reported, observed, physiologic, and analgesic outcomes. Drug Alcohol Depend. Rep. *8*, 100188. https://doi.org/10.1016/j.dadr.2023.100188.
6. Ren, Z.-Y., Xu, X.-Q., Bao, Y.-P., He, J., Shi, L., Deng, J.-H., Gao, X.-J., Tang, H.-L., Wang, Y.-M., and Lu, L. (2015). The impact of genetic variation on sensitivity to opioid analgesics in patients with postoperative pain: a systematic review and meta-analysis. Pain Physician *18*, 131–152.
7. Kaiko, R.F., Wallenstein, S.L., Rogers, A.G., and Houde, R.W. (1983). Sources of variation in analgesic responses in cancer patients with chronic pain receiving morphine. Pain *15*, 191–200. https://doi.org/10.1016/0304-3959(83)90018-0.
8. Dunn, K.E., Barrett, F.S., Brands, B., Marsh, D.C., and Bigelow, G.E. (2019). Individual differences in human opioid abuse potential as observed in a human laboratory study. Drug Alcohol Depend. *205*, 107688. https://doi.org/10.1016/j.drugalcdep.2019.107688.
9. Trang, T., Al-Hasani, R., Salvemini, D., Salter, M.W., Gutstein, H., and Cahill, C.M. (2015). Pain and Poppies: The Good, the Bad, and the Ugly of Opioid Analgesics. J. Neurosci. *35*, 13879–13888. https://doi.org/10.1523/JNEUROSCI.2711-15.2015.
10. Collett, B.J. (1998). Opioid tolerance: the clinical perspective. Br. J. Anaesth. *81*, 58–68. https://doi.org/10.1093/bja/81.1.58.
11. Chu, L.F., Angst, M.S., and Clark, D. (2008). Opioid-induced hyperalgesia in humans: molecular mechanisms and clinical considerations. Clin. J. Pain *24*, 479–496. https://doi.org/10.1097/AJP.0b013e31816b2f43.
12. Matic, M., de Wildt, S.N., Tibboel, D., and van Schaik, R.H.N. (2017). Analgesia and Opioids: A Pharmacogenetics Shortlist for Implementation in Clinical Practice. Clin. Chem. *63*, 1204–1213. https://doi.org/10.1373/clinchem.2016.264986.
13. De Gregori, M., Diatchenko, L., Ingelmo, P.M., Napolioni, V., Klepstad, P., Belfer, I., Molinaro, V., Garbin, G., Ranzani, G.N., Alberio, G., et al. (2016). Human Genetic Variability Contributes to Postoperative Morphine Consumption. J. Pain *17*, 628–636. https://doi.org/10.1016/j.jpain.2016.02.003.
14. Bugada, D., Lorini, L.F., Fumagalli, R., and Allegri, M. (2020). Genetics and Opioids: Towards More Appropriate Prescription in Cancer Pain. Cancers (Basel) *12*, 1951. https://doi.org/10.3390/cancers12071951.
15. Kosarac, B., Fox, A.A., and Collard, C.D. (2009). Effect of genetic factors on opioid action. Curr. Opin. Anaesthesiol. *22*, 476–482. https://doi.org/10.1097/ACO.0b013e32832e34c9.

16. Zhang, X., Jin, T., Wang, H., Han, S., and Liang, Y. (2024). Microglia in morphine tolerance: cellular and molecular mechanisms and therapeutic potential. Front. Pharmacol. *15*, 1499799. https://doi.org/10.3389/fphar.2024.1499799.

17. Leduc-Pessah, H., Weilinger, N.L., Fan, C.Y., Burma, N.E., Thompson, R.J., and Trang, T. (2017). Site-specific regulation of P2X7 receptor function in microglia gates morphine analgesic tolerance. J. Neurosci. *37*, 10154–10172. https://doi.org/10.1523/JNEUROSCI.0852-17.2017.

18. Tu, H., Chu, H., Guan, S., Hao, F., Xu, N., Zhao, Z., and Liang, Y. (2021). The role of the M1/M2 microglia in the process from cancer pain to morphine tolerance. Tissue Cell *68*, 101438. https://doi.org/10.1016/j.tice.2020.101438.

19. Horvath, R.J., and DeLeo, J.A. (2009). Morphine Enhances Microglial Migration through Modulation of P2X4 Receptor Signaling. J. Neurosci. *29*, 998–1005. https://doi.org/10.1523/JNEUROSCI.4595-08.2009.

20. Merighi, S., Gessi, S., Varani, K., Fazzi, D., Stefanelli, A., and Borea, P.A. (2013). Morphine mediates a proinflammatory phenotype via μ-opioid receptor–PKCε–Akt–ERK1/2 signaling pathway in activated microglial cells. Biochem. Pharmacol. *86*, 487–496. https://doi.org/10.1016/j.bcp.2013.05.027.

21. Cuitavi, J., Andrés-Herrera, P., Meseguer, D., Campos-Jurado, Y., Lorente, J.D., Caruana, H., and Hipólito, L. (2023). Focal mu-opioid receptor activation promotes neuroinflammation and microglial activation in the mesocorticolimbic system: Alterations induced by inflammatory pain. Glia *71*, 1906–1920. https://doi.org/10.1002/glia.24374.

22. Maduna, T., Audouard, E., Dembélé, D., Mouzaoui, N., Reiss, D., Massotte, D., and Gaveriaux-Ruff, C. (2019). Microglia Express Mu Opioid Receptor: Insights From Transcriptomics and Fluorescent Reporter Mice. Front. Psychiatry *9*, 726. https://doi.org/10.3389/fpsyt.2018.00726.

23. Mali, A.S., and Novotny, J. (2022). Opioid receptor activation suppresses the neuroinflammatory response by promoting microglial M2 polarization. Mol. Cell. Neurosci. *121*, 103744. https://doi.org/10.1016/j.mcn.2022.103744.

24. Eidson, L.N., and Murphy, A.Z. (2019). Inflammatory Mediators of Opioid Tolerance: Implications for Dependency and Addiction. Peptides *115*, 51–58. https://doi.org/10.1016/j.peptides.2019.01.003.

25. Grace, P.M., Maier, S.F., and Watkins, L.R. (2015). Opioid-Induced Central Immune Signaling: Implications for Opioid Analgesia. Headache *55*, 475–489. https://doi.org/10.1111/head.12552.

26. Green, J.M., Sundman, M.H., and Chou, Y.H. (2022). Opioid-induced microglia reactivity modulates opioid reward, analgesia, and behavior. Neurosci. Biobehav. Rev. *135*, 104544. https://doi.org/10.1016/j.neubiorev.2022.104544.

27. Hutchinson, M.R., Bland, S.T., Johnson, K.W., Rice, K.C., Maier, S.F., and Watkins, L.R. (2007). Opioid-Induced Glial Activation: Mechanisms of Activation and Implications for Opioid Analgesia, Dependence, and Reward. ScientificWorldJournal *7*, 98–111. https://doi.org/10.1100/tsw.2007.230.

28. Satoh, J.-I., Asahina, N., Kitano, S., and Kino, Y. (2014). A Comprehensive Profile of ChIP-Seq-Based PU.1/Spi1 Target Genes in Microglia. Gene Regul. Syst. Bio. *8*, 127–139. https://doi.org/10.4137/GRSB.S19711.

29. Zusso, M., Methot, L., Lo, R., Greenhalgh, A.D., David, S., and Stifani, S. (2012). Regulation of postnatal forebrain amoeboid microglial cell proliferation and development by the transcription factor Runx1. J. Neurosci. *32*, 11285–11298. https://doi.org/10.1523/JNEUROSCI.6182-11.2012.

30. Holtman, I.R., Skola, D., and Glass, C.K. (2017). Transcriptional control of microglia phenotypes in health and disease. J. Clin. Investig. *127*, 3220–3229. https://doi.org/10.1172/JCI90604.

31. Buttgereit, A., Lelios, I., Yu, X., Vrohlings, M., Krakoski, N.R., Gautier, E.L., Nishinakamura, R., Becher, B., and Greter, M. (2016). Sall1 is a transcriptional regulator defining microglia identity and function. Nat. Immunol. *17*, 1397–1406. https://doi.org/10.1038/ni.3585.

32. Kierdorf, K., and Prinz, M. (2013). Factors regulating microglia activation. Front. Cell. Neurosci. *7*, 44. https://doi.org/10.3389/fncel.2013.00044.

33. Yeh, H., and Ikezu, T. (2019). Transcriptional and epigenetic regulation of microglia in health and disease. Trends Mol. Med. *25*, 96–111. https://doi.org/10.1016/j.molmed.2018.11.004.

34. Krasemann, S., Madore, C., Cialic, R., Baufeld, C., Calcagno, N., El Fatimy, R., Beckers, L., O'Loughlin, E., Xu, Y., Fanek, Z., et al. (2017). The TREM2-APOE pathway drives the transcriptional phenotype of dysfunctional microglia in neurodegenerative diseases. Immunity *47*, 566–581.e9. https://doi.org/10.1016/j.immuni.2017.08.008.

35. Kierdorf, K., and Prinz, M. (2017). Microglia in steady state. J. Clin. Investig. *127*, 3201–3209. https://doi.org/10.1172/JCI90602.

36. Wehrspaun, C.C., Haerty, W., and Ponting, C.P. (2015). Microglia recapitulate a hematopoietic master regulator network in the aging human frontal cortex. Neurobiol. Aging *36*, 2443.e9–2443.e20. https://doi.org/10.1016/j.neurobiolaging.2015.04.008.

37. Cunningham, L., Finckbeiner, S., Hyde, R.K., Southall, N., Marugan, J., Yedavalli, V.R.K., Dehdashti, S.J., Reinhold, W.C., Alemu, L., Zhao, L., et al. (2012). Identification of benzodiazepine Ro5-3335 as an inhibitor of CBF leukemia through quantitative high throughput screen against RUNX1–CBFβ interaction. Proc. Natl. Acad. Sci. USA *109*, 14592–14597. https://doi.org/10.1073/pnas.1200037109.

38. Burma, N.E., Bonin, R.P., Leduc-Pessah, H., Baimel, C., Cairncross, Z.F., Mousseau, M., Shankara, J.V., Stemkowski, P.L., Baimoukhametova, D., Bains, J.S., et al. (2017). Blocking microglial pannexin-1 channels alleviates morphine withdrawal in rodents. Nat. Med. *23*, 355–360. https://doi.org/10.1038/nm.4281.

39. Burma, N.E., Leduc-Pessah, H., and Trang, T. (2017). Genetic deletion of microglial Panx1 attenuates morphine withdrawal, but not analgesic tolerance or hyperalgesia in mice. Channels (Austin) *11*, 487–494. https://doi.org/10.1080/19336950.2017.1359361.

40. Parkhurst, C.N., Yang, G., Ninan, I., Savas, J.N., Yates, J.R., Lafaille, J.J., Hempstead, B.L., Littman, D.R., and Gan, W.-B. (2013). Microglia promote learning-dependent synapse formation through brain-derived neurotrophic factor. Cell *155*, 1596–1609. https://doi.org/10.1016/j.cell.2013.11.030.

41. Coffey, K.R., Lesiak, A.J., Marx, R.G., Vo, E.K., Garden, G.A., and Neumaier, J.F. (2021). A cAMP-Related Gene Network in Microglia Is Inversely Regulated by Morphine Tolerance and Withdrawal. Biol. Psychiatry Glob. Open Sci. *2*, 180–189. https://doi.org/10.1016/j.bpsgos.2021.07.011.

42. Reiss, D., Maduna, T., Maurin, H., Audouard, E., and Gaveriaux-Ruff, C. (2020). Mu opioid receptor in microglia contributes to morphine analgesic tolerance, hyperalgesia, and withdrawal in mice. J. Neurosci. Res. *100*, 203–219. https://doi.org/10.1002/jnr.24626.

43. Chen, C.-L., Broom, D.C., Liu, Y., de Nooij, J.C., Li, Z., Cen, C., Samad, O.A., Jessell, T.M., Woolf, C.J., and Ma, Q. (2006). Runx1 determines nociceptive sensory neuron phenotype and is required for thermal and neuropathic pain. Neuron *49*, 365–377. https://doi.org/10.1016/j.neuron.2005.10.036.

44. Marmigère, F., Montelius, A., Wegner, M., Groner, Y., Reichardt, L.F., and Ernfors, P. (2006). The Runx1/AML1 transcription factor selectively regulates development and survival of TrkA nociceptive sensory neurons. Nat. Neurosci. *9*, 180–187. https://doi.org/10.1038/nn1631.

45. Kramer, I., Sigrist, M., de Nooij, J.C., Taniuchi, I., Jessell, T.M., and Arber, S. (2006). A role for Runx transcription factor signaling in dorsal root ganglion sensory neuron diversification. Neuron *49*, 379–393. https://doi.org/10.1016/j.neuron.2006.01.008.

46. Kobayashi, A., Senzaki, K., Ozaki, S., Yoshikawa, M., and Shiga, T. (2012). Runx1 promotes neuronal differentiation in dorsal root ganglion.

Mol. Cell. Neurosci. *49*, 23–31. https://doi.org/10.1016/j.mcn.2011.08.009.

47. Dorion, M.-F., Casas, D., Shlaifer, I., Yaqubi, M., Fleming, P., Karpilovsky, N., Chen, C.X.-Q., Nicouleau, M., Piscopo, V.E.C., MacDougall, E.J., et al. (2024). An adapted protocol to derive microglia from stem cells and its application in the study of CSF1R-related disorders. Mol. Neurodegener. *19*, 31. https://doi.org/10.1186/s13024-024-00723-x.
48. Dorion, M.-F., Yaqubi, M., Murdoch, H.J., Hall, J.A., Dudley, R., Antel, J.P., Durcan, T.M., and Healy, L.M. (2023). Systematic comparison of culture media uncovers phenotypic shift of primary human microglia defined by reduced reliance to CSF1R signaling. Glia *71*, 1278–1293. https://doi.org/10.1002/glia.24338.
49. Angst, M.S., Phillips, N.G., Drover, D.R., Tingle, M., Ray, A., Swan, G.E., Lazzeroni, L.C., and Clark, D.J. (2012). Pain sensitivity and opioid analgesia: a pharmacogenomic twin study. Pain *153*, 1397–1409. https://doi.org/10.1016/j.pain.2012.02.022.
50. Nishizawa, D., Fukuda, K., Kasai, S., Hasegawa, J., Aoki, Y., Nishi, A., Saita, N., Koukita, Y., Nagashima, M., Katoh, R., et al. (2014). Genome-wide association study identifies a potent locus associated with human opioid sensitivity. Mol. Psychiatry *19*, 55–62. https://doi.org/10.1038/mp.2012.164.
51. Hayashida, M., Nagashima, M., Satoh, Y., Katoh, R., Tagami, M., Ide, S., Kasai, S., Nishizawa, D., Ogai, Y., Hasegawa, J., et al. (2008). Analgesic requirements after major abdominal surgery are associated with OPRM1 gene polymorphism genotype and haplotype. Pharmacogenomics *9*, 1605–1616. https://doi.org/10.2217/14622416.9.11.1605.
52. Walter, C., and Lötsch, J. (2009). Meta-analysis of the relevance of the OPRM1 118A>G genetic variant for pain treatment. Pain *146*, 270–275. https://doi.org/10.1016/j.pain.2009.07.013.
53. Bond, C., LaForge, K.S., Tian, M., Melia, D., Zhang, S., Borg, L., Gong, J., Schluger, J., Strong, J.A., Leal, S.M., et al. (1998). Single-nucleotide polymorphism in the human mu opioid receptor gene alters β-endorphin binding and activity: Possible implications for opiate addiction. Proc. Natl. Acad. Sci. USA *95*, 9608–9613. https://doi.org/10.1073/pnas.95.16.9608.
54. Nelson, E.C., Lynskey, M.T., Heath, A.C., Wray, N., Agrawal, A., Shand, F.L., Henders, A.K., Wallace, L., Todorov, A.A., Schrage, A.J., et al. (2013). ANKK1, TTC12, and NCAM1 polymorphisms and heroin dependence: importance of considering drug exposure. JAMA Psychiatry *70*, 325–333. https://doi.org/10.1001/jamapsychiatry.2013.282.
55. Nelson, E.C., Lynskey, M.T., Heath, A.C., Wray, N., Agrawal, A., Shand, F.L., Henders, A.K., Wallace, L., Todorov, A.A., Schrage, A.J., et al. (2014). Association of OPRD1 polymorphisms with heroin dependence in a large case-control series. Addict. Biol. *19*, 111–121. https://doi.org/10.1111/j.1369-1600.2012.00445.x.
56. Baby, N., Li, Y., Ling, E.-A., Lu, J., and Dheen, S.T. (2014). Runx1t1 (Runt-Related Transcription Factor 1; Translocated to, 1) Epigenetically Regulates the Proliferation and Nitric Oxide Production of Microglia. PLoS One *9*, e89326. https://doi.org/10.1371/journal.pone.0089326.
57. Logan, T.T., Villapol, S., and Symes, A.J. (2013). TGF-β superfamily gene expression and induction of the Runx1 transcription factor in adult neurogenic regions after brain injury. PLoS One *8*, e59250. https://doi.org/10.1371/journal.pone.0059250.
58. Deng, X.-L., Feng, L., Wang, Z.-X., Zhao, Y.-E., Zhan, Q., Wu, X.-M., Xiao, B., and Shu, Y. (2020). The Runx1/Notch1 Signaling Pathway Participates in M1/M2 Microglia Polarization in a Mouse Model of Temporal Lobe Epilepsy and in BV-2 Cells. Neurochem. Res. *45*, 2204–2216. https://doi.org/10.1007/s11064-020-03082-3.
59. Masuda, T., Sankowski, R., Staszewski, O., Böttcher, C., Amann, L., Sagar, Scheiwe, C., Nessler, S., Kunz, P., van Loo, G., et al. (2019). Spatial and temporal heterogeneity of mouse and human microglia at single-cell resolution. Nature *566*, 388–392. https://doi.org/10.1038/s41586-019-0924-x.
60. Jurga, A.M., Paleczna, M., and Kuter, K.Z. (2020). Overview of General and Discriminating Markers of Differential Microglia Phenotypes. Front. Cell. Neurosci. *14*, 198. https://doi.org/10.3389/fncel.2020.00198.
61. Tan, Y.-L., Yuan, Y., and Tian, L. (2020). Microglial regional heterogeneity and its role in the brain. Mol. Psychiatry *25*, 351–367. https://doi.org/10.1038/s41380-019-0609-8.
62. Huang, S., O'Donovan, K.J., Turner, E.E., Zhong, J., and Ginty, D.D. (2015). Extrinsic and intrinsic signals converge on the Runx1/CBFβ transcription factor for nonpeptidergic nociceptor maturation. eLife *4*, e10874. https://doi.org/10.7554/eLife.10874.
63. Chen, Y., Bajpai, A.K., Li, N., Xiang, J., Wang, A., Gu, Q., Ruan, J., Zhang, R., Chen, G., and Lu, L. (2025). Discovery of Novel Pain Regulators Through Integration of Cross-Species High-Throughput Data. CNS Neurosci. Ther. *31*, e70255. https://doi.org/10.1111/cns.70255.
64. Phan, B.N., Ray, M.H., Xue, X., Fu, C., Fenster, R.J., Kohut, S.J., Bergman, J., Haber, S.N., McCullough, K.M., Fish, M.K., et al. (2024). Single nuclei transcriptomics in human and non-human primate striatum in opioid use disorder. Nat. Commun. *15*, 878. https://doi.org/10.1038/s41467-024-45165-7.
65. Tang, H., Zhang, Y., Xun, Y., Yu, J., Lu, Y., Zhang, R., Dang, W., Zhu, F., and Zhang, J. (2023). Association between methylation in the promoter region of the GAD2 gene and opioid use disorder. Brain Res. *1812*, 148407. https://doi.org/10.1016/j.brainres.2023.148407.
66. Radhakrishna, U., Radhakrishnan, R., Uppala, L.V., Trivedi, T.S., Prajapati, J., Rawal, R.M., Muvvala, S.B., Bahado-Singh, R.O., and Sadhasivam, S. (2025). Prenatal opioid exposure alters pain perception and increases long-term health risks in infants with neonatal opioid withdrawal syndrome. Front. Pain Res. (Lausanne) *6*, 1497801. https://doi.org/10.3389/fpain.2025.1497801.
67. Wang, Q., Stacy, T., Binder, M., Marin-Padilla, M., Sharpe, A.H., and Speck, N.A. (1996). Disruption of the Cbfa2 gene causes necrosis and hemorrhaging in the central nervous system and blocks definitive hematopoiesis. Proc. Natl. Acad. Sci. USA *93*, 3444–3449. https://doi.org/10.1073/pnas.93.8.3444.
68. Butler, A., Hoffman, P., Smibert, P., Papalexi, E., and Satija, R. (2018). Integrating single-cell transcriptomic data across different conditions, technologies, and species. Nat. Biotechnol. *36*, 411–420. https://doi.org/10.1038/nbt.4096.
69. Bolger, A.M., Lohse, M., and Usadel, B. (2014). Trimmomatic: a flexible trimmer for Illumina sequence data. Bioinformatics *30*, 2114–2120. https://doi.org/10.1093/bioinformatics/btu170.
70. Langmead, B., and Salzberg, S.L. (2012). Fast gapped-read alignment with Bowtie 2. Nat. Methods *9*, 357–359. https://doi.org/10.1038/nmeth.1923.
71. Untergasser, A., Cutcutache, I., Koressaar, T., Ye, J., Faircloth, B.C., Remm, M., and Rozen, S.G. (2012). Primer3–new capabilities and interfaces. Nucleic Acids Res. *40*, e115. https://doi.org/10.1093/nar/gks596.
72. Barrett, J.C., Fry, B., Maller, J., and Daly, M.J. (2005). Haploview: analysis and visualization of LD and haplotype maps. Bioinformatics *21*, 263–265. https://doi.org/10.1093/bioinformatics/bth457.
73. Mousseau, M., Burma, N.E., Lee, K.Y., Leduc-Pessah, H., Kwok, C.H.T., Reid, A.R., O'Brien, M., Sagalajev, B., Stratton, J.A., Patrick, N., et al. (2018). Microglial pannexin-1 channel activation is a spinal determinant of joint pain. Sci Adv. *4*, eaas9846. https://doi.org/10.1126/sciadv.aas9846.
74. Tang, Y.M., Pulimood, N.S., and Stifani, S. (2022). Comparing the Characteristics of Microglia Preparations Generated Using Different Human iPSC-Based Differentiation Methods to Model Neurodegenerative Diseases. ASN Neuro *14*, 17590914221145105. https://doi.org/10.1177/17590914221145105.
75. Douvaras, P., Sun, B., Wang, M., Kruglikov, I., Lallos, G., Zimmer, M., Terrenoire, C., Zhang, B., Gandy, S., Schadt, E., et al. (2017). Directed

Differentiation of Human Pluripotent Stem Cells to Microglia. Stem Cell Rep. *8*, 1516–1524. https://doi.org/10.1016/j.stemcr.2017.04.023.

76. Trang, T., Beggs, S., Wan, X., and Salter, M.W. (2009). P2X4-receptor-mediated synthesis and release of brain-derived neurotrophic factor in microglia is dependent on calcium and p38-mitogen-activated protein kinase activation. J. Neurosci. *29*, 3518–3528. https://doi.org/10.1523/JNEUROSCI.5714-08.2009.

77. Durafourt, B.A., Moore, C.S., Zammit, D.A., Johnson, T.A., Zaguia, F., Guiot, M.-C., Bar-Or, A., and Antel, J.P. (2012). Comparison of polarization properties of human adult microglia and blood-derived macrophages. Glia *60*, 717–727. https://doi.org/10.1002/glia.22298.

78. Durafourt, B.A., Moore, C.S., Blain, M., and Antel, J.P. (2013). Isolating, culturing, and polarizing primary human adult and fetal microglia. Methods Mol. Biol. *1041*, 199–211. https://doi.org/10.1007/978-1-62703-520-0_19.

79. Fukuda, K., Hayashida, M., Ide, S., Saita, N., Kokita, Y., Kasai, S., Nishizawa, D., Ogai, Y., Hasegawa, J., Nagashima, M., et al. (2009). Association between OPRM1 gene polymorphisms and fentanyl sensitivity in patients undergoing painful cosmetic surgery. Pain *147*, 194–201. https://doi.org/10.1016/j.pain.2009.09.004.

80. Nishizawa, D., Nagashima, M., Katoh, R., Satoh, Y., Tagami, M., Kasai, S., Ogai, Y., Han, W., Hasegawa, J., Shimoyama, N., et al. (2009). Association between KCNJ6 (GIRK2) gene polymorphisms and postoperative analgesic requirements after major abdominal surgery. PLoS One *4*, e7060. https://doi.org/10.1371/journal.pone.0007060.

81. Bucholz, K.K., Cadoret, R., Cloninger, C.R., Dinwiddie, S.H., Hesselbrock, V.M., Nurnberger, J.I., Reich, T., Schmidt, I., and Schuckit, M.A. (1994). A new, semi-structured psychiatric interview for use in genetic linkage studies: a report on the reliability of the SSAGA. J. Stud. Alcohol *55*, 149–158. https://doi.org/10.15288/jsa.1994.55.149.

82. De la Calle, J.L., and Paíno, C.L. (2002). A procedure for direct lumbar puncture in rats. Brain Res. Bull. *59*, 245–250. https://doi.org/10.1016/S0361-9230(02)00866-3.

83. D'amour, F.E., and Smith, D.L. (1941). A Method for Determining Loss of Pain Sensation. J. Pharmacol. Exp. Ther. *72*, 74–79. https://doi.org/10.1016/S0022-3565(25)03823-6.

84. Kwok, C.H.T., Harding, E.K., Burma, N.E., Markovic, T., Massaly, N., van den Hoogen, N.J., Stokes-Heck, S., Gambeta, E., Komarek, K., Yoon, H.J., et al. (2024). Pannexin-1 channel inhibition alleviates opioid withdrawal in rodents by modulating locus coeruleus to spinal cord circuitry. Nat Commun. *15*, 6264. https://doi.org/10.1038/s41467-024-50657-7.

85. Ferrini, F., Trang, T., Mattioli, T.-A.M., Laffray, S., Del'Guidice, T., Lorenzo, L.-E., Castonguay, A., Doyon, N., Zhang, W., Godin, A.G., et al. (2013). Morphine hyperalgesia gated through microglia-mediated disruption of neuronal Cl^- homeostasis. Nat. Neurosci. *16*, 183–192. https://doi.org/10.1038/nn.3295.

86. Pogatzki, E.M., and Raja, S.N. (2003). A mouse model of incisional pain. Anesthesiology *99*, 1023–1027. https://doi.org/10.1097/00000542-200310000-00041.

87. Bonin, R.P., Bories, C., and De Koninck, Y. (2014). A simplified up-down method (SUDO) for measuring mechanical nociception in rodents using von Frey filaments. Mol. Pain *10*, 26. https://doi.org/10.1186/1744-8069-10-26.

88. Ferreira, J., Campos, M.M., Pesquero, J.B., Araújo, R.C., Bader, M., and Calixto, J.B. (2001). Evidence for the participation of kinins in Freund's adjuvant-induced inflammatory and nociceptive responses in kinin B1 and B2 receptor knockout mice. Neuropharmacology *41*, 1006–1012. https://doi.org/10.1016/s0028-3908(01)00142-3.

89. Chaplan, S.R., Pogrel, J.W., and Yaksh, T.L. (1994). Role of voltage-dependent calcium channel subtypes in experimental tactile allodynia. J. Pharmacol. Exp. Ther. *269*, 1117–1123. https://doi.org/10.1016/S0022-3565(25)38848-8.

90. Decosterd, I., and Woolf, C.J. (2000). Spared nerve injury: an animal model of persistent peripheral neuropathic pain. Pain *87*, 149–158. https://doi.org/10.1016/S0304-3959(00)00276-1.

91. Dalgarno, R., Leduc-Pessah, H., Pilapil, A., Kwok, C.H., and Trang, T. (2018). Intrathecal delivery of a palmitoylated peptide targeting Y382-384 within the P2X7 receptor alleviates neuropathic pain. Mol. Pain *14*, 1744806918795793. https://doi.org/10.1177/1744806918795793.

92. St-Pierre, M.-K., Carrier, M., Lau, V., and Tremblay, M.-È. (2022). Investigating Microglial Ultrastructural Alterations and Intimate Relationships with Neuronal Stress, Dystrophy, and Degeneration in Mouse Models of Alzheimer's Disease. Methods Mol. Biol. *2515*, 29–58. https://doi.org/10.1007/978-1-0716-2409-8_3.

93. St-Pierre, M.-K., Carrier, M., González Ibáñez, F., Šimončičová, E., Wallman, M.-J., Vallières, L., Parent, M., and Tremblay, M.-È. (2022). Ultrastructural characterization of dark microglia during aging in a mouse model of Alzheimer's disease pathology and in human post-mortem brain samples. J. Neuroinflamm. *19*, 235. https://doi.org/10.1186/s12974-022-02595-8.

94. Schmittgen, T.D., and Livak, K.J. (2008). Analyzing real-time PCR data by the comparative C_T method. Nat. Protoc. *3*, 1101–1108. https://doi.org/10.1038/nprot.2008.73.

95. Sanz, E., Yang, L., Su, T., Morris, D.R., McKnight, G.S., and Amieux, P.S. (2009). Cell-type-specific isolation of ribosome-associated mRNA from complex tissues. Proc. Natl. Acad. Sci. USA *106*, 13939–13944. https://doi.org/10.1073/pnas.0907143106.

96. Fan, C.Y., McAllister, B.B., Stokes-Heck, S., Harding, E.K., Pereira de Vasconcelos, A., Mah, L.K., Lima, L.V., van den Hoogen, N.J., Rosen, S.F., Ham, B., et al. (2025). Divergent sex-specific pannexin-1 mechanisms in microglia and T cells underlie neuropathic pain. Neuron *113*, 896–911.e9. https://doi.org/10.1016/j.neuron.2025.01.005.

97. Stratton, J.A., Sinha, S., Shin, W., Labit, E., Chu, T.-H., Shah, P.T., Midha, R., and Biernaskie, J. (2019). Droplet Barcoding-Based Single Cell Transcriptomics of Adult Mammalian Tissues. J. Vis. Exp. e58709. https://doi.org/10.3791/58709.

98. Zheng, G.X.Y., Terry, J.M., Belgrader, P., Ryvkin, P., Bent, Z.W., Wilson, R., Ziraldo, S.B., Wheeler, T.D., McDermott, G.P., Zhu, J., et al. (2017). Massively parallel digital transcriptional profiling of single cells. Nat. Commun. *8*, 14049. https://doi.org/10.1038/ncomms14049.

99. Macosko, E.Z., Basu, A., Satija, R., Nemesh, J., Shekhar, K., Goldman, M., Tirosh, I., Bialas, A.R., Kamitaki, N., Martersteck, E.M., et al. (2015). Highly Parallel Genome-wide Expression Profiling of Individual Cells Using Nanoliter Droplets. Cell *161*, 1202–1214. https://doi.org/10.1016/j.cell.2015.05.002.

100. Ting, J.T., Daigle, T.L., Chen, Q., and Feng, G. (2014). Acute brain slice methods for adult and aging animals: application of targeted patch clamp analysis and optogenetics. Methods Mol. Biol. *1183*, 221–242. https://doi.org/10.1007/978-1-4939-1096-0_14.

101. Chéry, N., and de Koninck, Y. (1999). Junctional versus extrajunctional glycine and GABA(A) receptor-mediated IPSCs in identified lamina I neurons of the adult rat spinal cord. J. Neurosci. *19*, 7342–7355. https://doi.org/10.1523/JNEUROSCI.19-17-07342.1999.

102. Nishizawa, D., Fukuda, K., Kasai, S., Ogai, Y., Hasegawa, J., Sato, N., Yamada, H., Tanioka, F., Sugimura, H., Hayashida, M., et al. (2014). Association between KCNJ6 (GIRK2) gene polymorphism rs2835859 and post-operative analgesia, pain sensitivity, and nicotine dependence. J. Pharmacol. Sci. *126*, 253–263. https://doi.org/10.1254/jphs.14189FP.

103. Amano, K., Nishizawa, D., Mieda, T., Tsujita, M., Kitamura, A., Hasegawa, J., Inada, E., Hayashida, M., and Ikeda, K. (2016). Opposite Associations Between the rs3845446 Single-Nucleotide Polymorphism of the CACNA1E Gene and Postoperative Pain-Related Phenotypes in Gastrointestinal Surgery Versus Previously Reported Orthognathic Surgery. J. Pain *17*, 1126–1134. https://doi.org/10.1016/j.jpain.2016.07.001.

104. Gabriel, S.B., Schaffner, S.F., Nguyen, H., Moore, J.M., Roy, J., Blumenstiel, B., Higgins, J., DeFelice, M., Lochner, A., Faggart, M., et al. (2002). The structure of haplotype blocks in the human genome. Science *296*, 2225–2229. https://doi.org/10.1126/science.1069424.

105. de Bakker, P.I.W., Yelensky, R., Pe'er, I., Gabriel, S.B., Daly, M.J., and Altshuler, D. (2005). Efficiency and power in genetic association studies. Nat. Genet. *37*, 1217–1223. https://doi.org/10.1038/ng1669.

106. Nelson, E.C., Agrawal, A., Heath, A.C., Bogdan, R., Sherva, R., Zhang, B., Al-Hasani, R., Bruchas, M.R., Chou, Y.L., Demers, C.H., et al. (2016). Evidence of CNIH3 involvement in opioid dependence. Mol. Psychiatry *21*, 608–614. https://doi.org/10.1038/mp.2015.102.

107. Manly, B.F.J., Navarro-Alberto, J.A. (2021). Randomization, Bootstrap and Monte Carlo Methods in Biology. Fourth Edition. https://www.routledge.com/Randomization-Bootstrap-and-Monte-Carlo-Methods-in-Biology/Manly-NavarroAlberto/p/book/9780367512873.

108. Hochberg, Y. (1988). A Sharper Bonferroni Procedure for Multiple Tests of Significance. Biometrika *75*, 800–802. https://doi.org/10.2307/2336325.

109. Toomaj, A., Sunoj, S.M., and Navarro, J. (2017). Some Properties of the Cumulative Residual Entropy of Coherent and Mixed Systems. J. Appl. Probab. *54*, 379–393. https://doi.org/10.1017/jpr.2017.6.

110. Rao, M., Chen, Y., Vemuri, B.C., and Wang, F. (2004). Cumulative residual entropy: a new measure of information. IEEE Transactions on Information Theory *50*, 1220–1228. https://ieeexplore.ieee.org/document/1302300.

111. Efron, B., and Tibshirani, R.J. (1994). An Introduction to the Bootstrap (Chapman and Hall/CRC). https://doi.org/10.1201/9780429246593.

112. Phipson, B., and Smyth, G.K. (2010). Permutation P-values should never be zero: calculating exact P-values when permutations are randomly drawn. Stat. Appl. Genet. Mol. Biol. *9*, 1. https://doi.org/10.2202/1544-6115.1585.

113. Patterson, N., Price, A.L., and Reich, D. (2006). Population structure and eigenanalysis. PLoS Genet. *2*, e190. https://doi.org/10.1371/journal.pgen.0020190.

114. Purcell, S., Neale, B., Todd-Brown, K., Thomas, L., Ferreira, M.A.R., Bender, D., Maller, J., Sklar, P., de Bakker, P.I.W., Daly, M.J., et al. (2007). PLINK: a tool set for whole-genome association and population-based linkage analyses. Am. J. Hum. Genet. *81*, 559–575. https://doi.org/10.1086/519795.

115. Benjamini, Y., and Hochberg, Y. (1995). Controlling the False Discovery Rate: A Practical and Powerful Approach to Multiple Testing. J. R. Stat. Soc., B (Methodol.) *57*, 289–300. https://doi.org/10.1111/j.2517-6161.1995.tb02031.x.

Please cite this article in press as: Leduc-Pessah et al., Runx1 transcription factor modulates opioid analgesia and withdrawal in humans and rodents, Neuron (2025), https://doi.org/10.1016/j.neuron.2025.11.018

STAR★METHODS

KEY RESOURCES TABLE

REAGENT or RESOURCE	SOURCE	IDENTIFIER
Antibodies		
Anti-CD11b/c (clone OX42), mouse, PE-conjugated	Thermo Fisher Scientific	Cat# 12-0110-82; RRID: AB_11150971
Anti-rat CD11b (clone OX-42), mouse	EMD Millipore	Cat# CBL1512; RRID: AB_93253
Anti-mouse CD11b (clone M1/70), rat	Abcam	Cat# ab8878; RRID: AB_306831
Anti-Runx1 (clone EPR3099), rabbit	Abcam	Cat# ab92336; RRID: AB_2049267
Anti-Ki67 (clone SP6), rabbit	Abcam	Cat# ab16667; RRID: AB_302459
Anti-Iba1, rabbit	Wako	Cat# 019-19741; RRID: AB_839504
Anti-F4/80 (clone CI:A3-1), rat	Abcam	Cat# ab6640; RRID: AB_1140040
Anti-CD68 (clone ED1), mouse	Abcam	Cat# ab31630; RRID: AB_1141557
Anti-CD45 (clone 2Q1384), mouse	Abcam	Cat# ab65274; RRID: AB_1140876
Anti-PU.1, rabbit	Cell Signaling Technology	Cat# 2266; RRID: AB_10692379
Anti-μ-opioid receptor, rabbit	Alomone Labs	Cat# AOR-011; RRID: AB_2040044
Anti-β-actin, mouse	Sigma-Aldrich	Cat# A5316; RRID: AB_476743
β-Tubulin III, rabbit	Sigma-Aldrich	Cat# T2200; RRID: AB_262133
Anti-Runx1, rabbit	Abcam	Cat# ab23980; RRID: AB_2184205
Biological samples		
Whole blood from orthognathic surgery patients	Nishizawa et al.[50]	N/A
Whole blood/oral mucosa samples from major abdominal surgery patients	Hayashida et al.[51]	N/A
DNA samples from Comorbidity and Trauma Study patients	Nelson et al.[54,55]	N/A
Chemicals, peptides, and recombinant proteins		
Morphine sulfate	PCCA; TRC	Cat# 20-1000; Cat# M652290
Ro5-3335	Tocris Bioscience	Cat# 4694
Tamoxifen	Sigma	Cat# T5648
Naloxone hydrochloride dihydrate	Sigma	Cat# N7758
Complete Freund's Adjuvant	Sigma	Cat# F5881
Critical commercial assays		
Mouse 31-plex cytokine array/ chemokine array	Eve Technologies	N/A
RNAscope 2.5 HD Assay-RED	Advanced Cell Diagnostics	Cat# 322350
SimpleChIP Enzymatic Chromatin IP Kit	Cell Signaling Technology	Cat# 9003
NEBNext Ultra DNA Library Preparation Kit	New England Biolabs	Cat# E7370L
Deposited data		
Single-cell RNA sequencing (scRNA-seq) and chromatin-immunoprecipitation sequencing (ChIP-seq) data	This paper	GEO: GSE253853
Experimental models: Cell lines		
Mouse: BV2	M. Tsuda, Kyushu University; K. Biber, University of Freiberg	RRID: CVCL_0182
Human: NCRM-1	National Institutes of Health Stem Cell Resource	RRID: CVCL_1E71
Human: CS52iALS-C9n6.ISOxx (CS52)	Cedars-Sinai Medical Center	RRID: CVCL_JC27

(*Continued on next page*)

Please cite this article in press as: Leduc-Pessah et al., Runx1 transcription factor modulates opioid analgesia and withdrawal in humans and rodents, Neuron (2025), https://doi.org/10.1016/j.neuron.2025.11.018

Continued

REAGENT or RESOURCE	SOURCE	IDENTIFIER
Human: CS29iALS-C9n1.ISOxx (CS29)	Cedars-Sinai Medical Center	RRID: CVCL_W559
Experimental models: Organisms/strains		
Rat: Sprague Dawley	Charles River	RRID: RGD_734476
Mouse: B6.129P2(Cg)-*Cx3cr1*$^{tm2.1(cre/ERT)Litt}$/WganJ (*Cx3cr1*-Cre^{ERT2})	The Jackson Laboratory	RRID: IMSR_JAX:021160
Mouse: *Runx1*^{tm1Spe} (Runx1$^{flx/flx}$)	N. A. Speck, University of Pennsylvania[67]	N/A
Mouse: B6N.129-*Rpl22*$^{tm1.1Psam}$/J(RiboTag)	The Jackson Laboratory	RRID: IMSR_JAX:011029
Mouse: C57BL/6J	The Jackson Laboratory	RRID: IMSR_JAX:000664
Oligonucleotides		
See Table S1 for qPCR Primer Sequences	This study	N/A
RNAscope *Oprm1* probe, mouse	Advanced Cell Diagnostics	Cat# 315841
TaqMan *RUNX1* SNP genotyping probe, Assay ID: C___2184062_10	Thermo Fisher Scientific	Cat# 4351379
Software and algorithms		
ImageJ (multiple versions)	NIH	https://imagej.net/ij/download.html
Prism (versions 6 and 10)	GraphPad Software	https://www.graphpad.com/
EZC1	Nikon	N/A
NIS-Elements	Nikon	https://www.microscope.healthcare.nikon.com/products/software/nis-elements
Cell Ranger (version 2.1.0)	10x Genomics	https://www.10xgenomics.com/support/software/cell-ranger/downloads
Seurat (version 2.3.4)	Satija Lab, New York Genome Center[68]	https://satijalab.org/seurat/articles/install.html
bcl2fastq (version 2.17)	Illumina	https://support.illumina.com/sequencing/sequencing_software/bcl2fastq-conversion-software/downloads.html
Trimmomatic (version 0.38)	Bolger et al., RWTH Aachen University[69]	http://www.usadellab.org/cms/?page=trimmomatic
bowtie2	Langmead et al., Johns Hopkins University[70]	https://bowtie-bio.sourceforge.net/bowtie2/index.shtml
Picard (version 2.18.26)	Broad Institute	https://broadinstitute.github.io/picard/
MACS2 (version 2.1.2)	Tao Liu	https://pypi.org/project/MACS2/
Primer3	Untergasser et al., Whitehead Institute for Biomedical Research[71]	https://primer3.ut.ee/
QuantStudio Design & Analysis (version 2.6.0)	Thermo Fisher Scientific	https://www.thermofisher.com/ca/en/home/technical-resources/software-downloads/quantstudio-3-5-real-time-pcr-systems.html
Clampex (version 10.2) and Clampfit (10.7)	Molecular Devices	https://support.moleculardevices.com/s/article/Axon-pCLAMP-10-Electrophysiology-Data-Acquisition-Analysis-Software-Download-Page
Clampex (version 11) and Clampfit (version 11)	Molecular Devices	https://support.moleculardevices.com/s/article/Axon-pCLAMP-11-Electrophysiology-Data-Acquisition-Analysis-Software-Download-Page
MiniAnalysis	Synaptosoft	RRID: SCR_002184
MATLAB (version 9.4.0)	MathWorks	https://www.mathworks.com/support/requirements/previous-releases.html
Easy Electrophysiology	Easy Electrophysiology Ltd	https://www.easyelectrophysiology.com/

(*Continued on next page*)

Please cite this article in press as: Leduc-Pessah et al., Runx1 transcription factor modulates opioid analgesia and withdrawal in humans and rodents, Neuron (2025), https://doi.org/10.1016/j.neuron.2025.11.018

Continued

REAGENT or RESOURCE	SOURCE	IDENTIFIER
Haploview (version 4.1)	Daly Lab, Broad Institute[72]	https://www.broadinstitute.org/haploview/haploview
BeadStudio	Illumina	https://www.illumina.com/Documents/products/datasheets/datasheet_beadstudio.pdf
GenomeStudio	Illumina	https://support.illumina.com/array/array_software/genomestudio/downloads.html
SPSS (version 25)	IBM	https://www.ibm.com/support/pages/downloading-ibm-spss-statistics-25
SmartPCA	Patterson et al., Broad Institute[72]	https://reich.hms.harvard.edu/software

EXPERIMENTAL MODEL AND STUDY PARTICIPANT DETAILS

Animals

Housing

All experiments were approved by the University of Calgary and Université Laval Animal Care Committees and are in accordance with the guidelines of the Canadian Council on Animal Care and the National Institutes of Health Guide for the Care and Use of Laboratory Animals. Male and female Sprague Dawley rats aged 7-9 weeks were purchased from Charles River (Sherbrooke, QC, Canada, RRID: RGD_734476). Rats were group housed 2 per cage, and cages were randomly assigned to experimental group. Male C57BL/6J mice (stock #000664, RRID: IMSR_JAX:000664) were obtained from the Jackson Laboratory (Bar Harbor, ME, USA). Other mouse lines were bred and maintained at the University of Calgary Clara Christie Centre for Mouse Genomics and Animal Resource Centre facilities. Mice were group housed with same-sex littermates, up to 5 per cage. All animals were housed under a 12-h:12-h light/dark cycle with *ad libitum* access to food and water. For mouse experiments, same-sex littermates from multiple litters of approximately the same age were used to reach the target sample size per experiment. Individual mice were randomly assigned to experimental group by a non-experimenter. Experimenters were blinded to genotype of animals and to tamoxifen or control treatment, as well as to drug treatment. Animals involved in each experiment were naïve to any previous drug administration or behavioral testing.

Cx3cr1-*Cre*^{ERT2}::Runx1$^{flx/flx}$ *mice*

To obtain a selective deletion of *Runx1* in microglia, a cre-loxP system was used. Mice expressing Cre-ERT2 fusion protein and EYFP under the *Cx3cr1* promoter (Jax mice: B6.129P2(Cg)-*Cx3cr1*$^{tm2.1(cre/ERT)Litt}$/WganJ, stock #021160, RRID: IMSR_JAX:021160) were crossed with *Runx1*$^{flx/flx}$ homozygote mice containing loxP sequences flanking exon 4 of the *Runx1* gene (*Runx1*^{tm1Spe}, generously donated from Dr. Nancy Speck's laboratory at the University of Pennsylvania).[67] Progeny genotype was screened using PCR, and mice were bred and backcrossed for 8 generations to yield the conditional knockout mice on a C57BL/6J background. Mice with an inducible knockout of Runx1 in CX_3CR_1-expressing cells (*Cx3cr1*-Cre$^{ERT2+/-}$::*Runx1*$^{flx/flx}$) and mice with no Cre expression (*Cx3cr1*-Cre$^{ERT2-/-}$::*Runx1*$^{flx/flx}$, abbreviated as *Runx1*$^{flx/flx}$) were used in experiments. To induce Cre recombination, mice were injected intraperitoneally with 1 mg of tamoxifen (Sigma, T5648) daily for 5 days or vehicle (sunflower oil with 10% ethanol) as a control. Tamoxifen-related effects were controlled for using mice lacking Cre expression (*Runx1*$^{flx/flx}$ littermate mice) that received 5 days of tamoxifen injections. Behavioral assessments and/or tissue collection were conducted 28 days after the first tamoxifen injection to allow for the repopulation of peripheral CX_3CR_1-expressing cells.[40]

Confirmation of recombination was assessed using PCR with a shared forward primer (Runx1-F; sequence: CCCACTG TGTGCATTCCAGATTGG) and an R1 reverse primer prior to the floxed region (Runx1-R1; sequence: GCTTCACTCTGACCAT CACCGTC; expected amplicon size: 275 bp) and R2 beyond the floxed region (Runx1-R2; sequence: CTGCACCCAGAAGCTAT GGTG; expected amplicon size: 1145 bp intact, 310 bp post-deletion).

Cx3cr1-*Cre*^{ERT2}::Rpl22^{HA} *mice*

Microglia-specific RiboTag mice were generated by crossing homozygous RiboTag mice (*Rpl22*^{HA}, The Jackson Laboratory, stock #011029, RRID: IMSR_JAX:011029) with homozygous *Cx3cr1*-Cre^{ERT2} mice to generate *Cx3Cr1*-Cre^{ERT2}::*Rpl22*^{HA} mice.[73] To induce recombination, mice were treated with tamoxifen (1 mg, intraperitoneal) over 5 days.

Cell lines

BV2 microglia culture

BV2 microglia-like cells (mouse-derived, female, CLS ATL03001, RRID: CVCL_0182) were provided by Drs. Makoto Tsuda and Knut Biber and were maintained in Dulbecco's Modified Eagle Medium (DMEM; Gibco) containing 5% fetal bovine serum (FBS), 1% penicillin-streptomycin (P/S) at 37°C with 5% CO_2. Cells were treated daily with morphine (1 μM or 10 μM) or saline, or Ro5 (0.5 μM) or control, for 5 days. After 5 days of drug treatment, BV2 cells were prepared for western blot, qPCR, or cytokine array analysis.

Please cite this article in press as: Leduc-Pessah et al., Runx1 transcription factor modulates opioid analgesia and withdrawal in humans and rodents, Neuron (2025), https://doi.org/10.1016/j.neuron.2025.11.018

iPSC-derived microglia cultures

Human induced pluripotent stem cell (iPSC) lines were induced into a microglial-like state as described by Tang et al.[74] Briefly, three separate human iPSC lines were used to ensure successful and reproducible generation of microglia. Cell lines included NCRM-1 (male, RRID: CVCL_1E71), CS52 (male, RRID: CVCL_JC27) and CS29 (male, RRID: CVCL_W559). Derivation of microglia was modified from methods described by Douvaras et al.[75] iPSCs were plated and maintained in Essential 6 Medium (ThermoFisher Scientific; A1516401) containing 80 ng/ml BMP4 (R&D Systems; Minneapolis, MN, USA; Cat No. 314-BPE) for 2–4 days until they reached near confluence. BMP4 signalling induced primitive hemangioblasts, and $CD45^{+}CX_3CR_1^{-}$ microglial progenitors appeared in the supernatant by day 16. Microglial progenitors were routinely collected as floating cells. Progenitors were cultured for further differentiation in SF-Microglia Medium (RPMI + IL-34 + GM-CSF). Cells were harvested and seeded onto 6-well plates in STEMdiff Hematopoietic kit (STEMCELL Technologies, 05310) medium for differentiation. Multiple ($n \geq 10$) cultures of each type of microglia preparation were generated and validated through morphological analysis and immunocytochemistry, and further plates were prepared for immunostaining.

Primary cell cultures

Rat microglia

Primary microglia cultures were prepared as described previously.[76] In brief, mixed glial culture was isolated from postnatal (P1-P3) male and female Sprague Dawley rat cortex or spinal cord and maintained for 10-14 days in DMEM containing 10% FBS and 1% P/S at 37°C with 5% CO_2. Microglia separated from the mixed culture by gentle shaking were plated and maintained with media changes every 2-3 days. Cells were treated with morphine (10 μM) or saline, or Ro5 (0.5 uM) or control, for 5 days and prepared for Western blot analysis, qPCR, immunocytochemistry, or chromatin immunoprecipitation.

Mouse dorsal root ganglion (DRG) neurons

DRG neurons were obtained from vehicle and tamoxifen treated *Cx3cr1*-Cre^{ERT2}::*Runx1*$^{flx/flx}$ male mice and underwent enzymatic dissociation in HBSS supplemented with 2 mg/ml collagenase type I and 4 mg/ml dispase (both sourced from Invitrogen) for 45 min at 37°C. Following dissociation, DRGs were washed twice in HBSS and once in Neurobasal A culture medium (Thermo Fisher Scientific) containing 2% B-27 supplement, 10% heat-inactivated FBS, 100 μg/ml streptomycin, 100 U/ml penicillin, 50 ng/ml nerve growth factor (NGF), and 50 ng/ml glial cell-derived neurotrophic factor (GDNF) (all obtained from Invitrogen). Individual neurons were isolated through trituration using a fire-polished glass Pasteur pipette in 4 ml of media and cultured overnight at 37°C with 5% CO_2 in 95% humidity on glass coverslips pre-coated with Poly-Ornithine and Laminin (both from Sigma-Aldrich).

Human microglia

Human microglia were isolated from adult male or female brain tissue, obtained from surgical resections from pharmacologically intractable non-malignant cases of temporal lobe epilepsy, using previously described protocols.[77,78] The tissue was provided from outside of the suspected focal site of epilepsy-related pathology. All procedures were carried out in accordance with the guidelines set by the Biomedical Ethics Unit of McGill University and approved under reference ANTJ2001/1. All experiments were conducted in accordance with the Helsinki Declaration, with sample procured with informed consent. Briefly, tissue was obtained in pieces <1 mm^3 and treated with DNase (Roche, Nutley, NJ) and trypsin (Invitrogen, Carlsbad, CA) for 30 min at 37°C. Following dissociation through a nylon mesh (37 μm), the cell suspension was separated on a 30% Percoll gradient (GE Healthcare, Piscataway, NJ) at 31,000 g for 30 min. Glial cells (oligodendrocytes and microglia) were collected from underneath the myelin layer, washed and plated at a density of 2 x 10^6 cells/ml in tissue-culture flasks. After 24 h in culture, microglia were separated based on differential adhesion properties of the cells. Microglia were subsequently grown for 4 days in flasks before gentle collection using 2 mM EDTA (Sigma-Aldrich), then plated in minimum essential medium (MEM, Sigma-Aldrich) supplemented with 5% FBS, 0.1% P/S, and 0.1% L-glutamine at a density of 5 x 10^5 cells/ml. Cells were treated with Ro5 (0.5 μM) or control as described and collected for qPCR. Additional experiments involved treating microglia with morphine (1 μM or 10 μM) or vehicle (PBS) for 5 consecutive days, after which cells were collected for qPCR or western blot.

Human participants

Painful cosmetic surgery patients

The protocol was approved by the Ethics Committees of Tokyo Dental College and the Tokyo Metropolitan Institute of Medical Science (approval no. 086 and 15-6, respectively) and conformed with the provisions of the Declaration of Helsinki. Written informed consent was obtained from all patients and from the parents if the patient was younger than 20 years old. The study included 355 healthy patients (American Society of Anesthesiologists Physical Status I, 15-50 years old, 125 males and 230 females) who were scheduled to undergo an orthognathic surgery, bilateral mandibular sagittal split ramus osteotomy (i.e., bilateral SSRO), for mandibular prognathism at Tokyo Dental College Suidobashi Hospital, detailed in previous reports.[79] All of the patients originated from Japan. Patients were excluded preoperatively if they had a history of acute or chronic kidney injury, drug abuse, or chronic pain or were unable to use the intravenous patient-controlled analgesia (IV-PCA) device.

The patients were orally premedicated with 5 mg diazepam and 150 mg famotidine 90 min before the induction of anesthesia. General anesthesia was induced with propofol at a target blood concentration of 4-6 μg/ml using a target-controlled infusion (TCI) pump (TE-317, Terumo, Tokyo, Japan). Vecuronium (0.1 mg/kg) was administered to facilitate nasotracheal intubation (Portex; inner diameter, 6.5-8.0 mm; Smiths Medical Japan, Tokyo, Japan) and maintained at 0.08 mg/kg/h during surgery. Whenever systolic blood

Please cite this article in press as: Leduc-Pessah et al., Runx1 transcription factor modulates opioid analgesia and withdrawal in humans and rodents, Neuron (2025), https://doi.org/10.1016/j.neuron.2025.11.018

pressure or heart rate increased more than 20% over baseline during surgery, fentanyl was intravenously administered at 1 μg/kg. The lungs were ventilated with oxygen-enriched air. All of the patients received local anesthesia at the surgical sites with 8 mL of 2% lidocaine that contained 12.5 μg/mL epinephrine. At the end of surgery, 50 mg rectal diclofenac sodium and 8 mg intravenous dexamethasone were administered to prevent postoperative orofacial edema/swelling. After emergence from anesthesia and tracheal extubation, 1.25 mg droperidol was intravenously administered to prevent nausea/vomiting, and IV-PCA with 20 μg/mL fentanyl commenced using a CADD-Legacy PCA pump (Smiths Medical Japan, Tokyo, Japan). Continuous background infusion was not employed. Patient-controlled analgesia was continued for 24 h postoperatively. In the case of refractory adverse effects or inadequate analgesia, PCA with fentanyl was discontinued, and 50 mg rectal diclofenac sodium was prescribed as a rescue analgesic as required. Postoperative fentanyl use (μg/kg) for 24 h was calculated based on PCA pump records. The intensity of spontaneous pain was assessed 24 h postoperatively using a 100 mm visual analog scale (VAS), with 0 mm indicating no pain and 100 mm indicating the worst pain imaginable. Perioperative (i.e., intraoperative + postoperative) fentanyl use was calculated, and 1 mg/kg of diclofenac sodium was converted to the fentanyl equivalent dose of 1 μg/kg, as were detailed in a previous report.[79] Total perioperative analgesic use was then calculated as the sum of perioperative fentanyl use and the fentanyl equivalent dose of diclofenac sodium. All of the doses of analgesics that were administered intraoperatively and postoperatively were normalized to body weight.

Major abdominal surgery patients

The study protocol was approved by the Institutional Review Boards at the Institute of Medical Science, Toho University Sakura Medical Center, and Tokyo Institute of Psychiatry (currently Tokyo Metropolitan Institute of Medical Science). All of the subjects provided informed, written consent for the genetic studies. Included in the study were 112 unrelated patients (age 28-80 years, 60 males and 52 females) who were scheduled to undergo major open abdominal surgery (OAS) for gastric cancer or open colectomy for colon cancer at the Research Hospital, Institute of Medical Science, The University of Tokyo, or Toho University Sakura Medical Center, during the period from January 2002 to December 2004.[51] All of the patients originated from Japan. Postoperative pain was managed by a combination of epidural analgesia infused at a constant rate and rescue analgesics. Peripheral blood or oral mucosa samples were collected for gene analysis.

Details for anesthesia, surgery, and postoperative pain management are described in a previous report.[51] Briefly, open gastrectomy or colectomy was performed under a combination of general and epidural anesthesia.[51] A lower thoracic or upper lumbar epidural catheter was placed before the induction of general anesthesia. General anesthesia was induced with oxygen, 1-2 mg/kg propofol, and 100 μg fentanyl. Vecuronium was administered as appropriate to facilitate intubation and surgery. General anesthesia was maintained with oxygen-enriched air and sevoflurane. A single dose of 6 mL of 0.5% bupivacaine with fentanyl or morphine was administered through the epidural catheter before surgery. Additional dosages of epidural local anesthetic were administered intermittently according to the preceding state of surgery. Postoperative pain was managed primarily with continuous epidural analgesia, which was started before emergence from anesthesia. Fentanyl or morphine was diluted with 0.25% bupivacaine in a total volume of 100 mL and infused at a constant rate of 2 mL/h. Whenever the patient complained of significant postoperative pain despite continuous epidural analgesia, appropriate doses of opioids and/or nonsteroidal anti-inflammatory drugs (NSAIDs) were administered as rescue analgesics. The frequency and doses of rescue analgesics, highest pain scores in numerical rating scale (NRS) using a 5-point numerical rating scale (0, no pain; 4, most severe pain imaginable), and doses of opioids that were infused epidurally during the first 24-h postoperative period were recorded. The doses of rescue analgesics that were administered during the first 24-h postoperative period were converted to equivalent doses of systemic fentanyl.[51,80]

Comorbidity and Trauma Study

The Comorbidity and Trauma Study (CATS) is a case-control genetic association study of opioid dependence (for detailed descriptions of CATS methods, see Nelson et al.[54,55]). Current analyses focused on CATS opioid dependent cases, aged 18 or older, who were recruited from clinics in the greater Sydney region at which they received opioid substitution therapy. Written informed consent was obtained from all participants as approved by the institutional review boards of the participating institutions. Semi-structured psychiatric diagnostic interviews, modified from the Semi-Structured Assessment for the Genetics of Alcoholism - Australia (SSAGA-OZ)[81] and completed in-person, provided a DSM-IV diagnosis of opioid dependence that included assessment of 15 opioid withdrawal symptoms. CATS European ancestry (EA) cases (n = 1226) were 60.1% male and had a mean age at interview of 36.7 years (SD 8.5).

METHOD DETAILS

Rodent surgeries and behavioral testing

Intrathecal drug administration

In rats, Ro5-3335 (Ro5, 15 μg, Tocris, Bristol, UK), a Runx1 inhibitor, was administered by intrathecal injection, under light anesthetic with 2% isoflurane (vol/vol), by lumbar puncture as previously described.[82] In mice, Ro5 was administered by intrathecal injection without anesthesia. Ro5 was administered once daily for 3 days prior to morphine treatment or tissue collection. For rats, Ro5 was reconstituted in 0.9% saline with 0.2% dimethyl sulfoxide (DMSO). For mice, Ro5 was reconstituted in 0.9% saline with 20% propylene glycol and 0.02% DMSO. All control animals received an equivalent volume of the appropriate vehicle.

Please cite this article in press as: Leduc-Pessah et al., Runx1 transcription factor modulates opioid analgesia and withdrawal in humans and rodents, Neuron (2025), https://doi.org/10.1016/j.neuron.2025.11.018

Acute morphine time-course and dose response

Morphine sulfate (MS; PCCA, London, ON, Canada, 20-1000; or TRC, Toronto, ON, Canada, M652290) prepared in 0.9% sterile saline solution was administered by intraperitoneal injection (rats: 15 mg/kg; mice: 10 mg/kg). In rats, acute morphine administration followed 3 days of intrathecal drug treatment with Ro5 or control, and thermal nociceptive threshold was assessed using the tail-flick test via application of an infrared thermal stimulus (Ugo Basile, Varese, Italy) to the ventral surface of the tail.[83] In mice, thermal nociceptive threshold was assessed using the tail-immersion test, where the distal portion of the tail is submerged in a 50°C water bath. In both assays, a 10-s cut-off time was used to prevent tissue damage. A time-course of morphine-induced antinociception was performed, with nociceptive testing at 30, 45, 60, 90 and 120 min after a single injection of morphine. Nociceptive measurements were normalized to baseline thresholds and presented as a percentage of the maximum possible effect (%MPE).

Morphine dose response was performed to determine morphine potency (ED_{50}). Ascending doses of morphine (2.5, 5, 10, 15, 20, 40 mg/kg) were given at 30-min intervals until a maximal level of antinociception was reached. Nociceptive measurements were taken 30 min after each morphine injection, normalized to baseline and presented as %MPE. The ED_{50} value was calculated using a non-linear regression in GraphPad Prism (version 6) software.

Hot plate test

Male and female Sprague Dawley rats were injected intraperitoneally with morphine (10 mg/kg). Rats were tested prior to morphine injection (baseline) and 30 min after injection. Rats were placed in a glass cylinder on a hot plate set to 52°C. The latency to reaction (paw licking or jumping), to a maximum of 20 s, was recorded by an observer blinded to the experimental treatment. The apparatus was cleaned with ethanol between animals.

Morphine tolerance

Morphine was administered to mice by intraperitoneal injection (10 mg/kg) once daily for 7 days. Thermal nociceptive threshold was assessed using the 50°C tail-immersion test, with a 10-s cut-off. Nociceptive measurements were taken prior to and 30 min after each morphine injection, normalized to daily baseline measurement and presented as %MPE.

Morphine-induced hyperalgesia

Mice received ascending doses of morphine intraperitoneally twice daily at 8-12 h intervals (day 1, 10 mg/kg; day 2, 20 mg/kg; day 3, 30 mg/kg; days 4 and 5, 40 mg/kg). Control mice received equivalent volumes of 0.9% saline twice daily. Thermal nociceptive threshold was assessed using a 48°C tail-immersion test, with a maximum cut-off time of 30 s to prevent tissue damage. Nociceptive thresholds were measured each day before the a.m. morphine injection and at least 12 h after the previous morphine injection to assess change in the baseline threshold.

Morphine withdrawal

Mice received ascending doses of morphine intraperitoneally twice daily at 8-h intervals (day 1, 7.5 and 15 mg/kg; day 2, 20 and 25 mg/kg; day 3, 30 and 35 mg/kg; day 4, 40 and 45 mg/kg).[84] On day 5, mice received a morning injection of morphine at 50 mg/kg and 2 h later naloxone (2 mg/kg, naloxone hydrochloride dihydrate, Sigma, N7758) to rapidly induce opioid withdrawal. Control mice received an equivalent volume of 0.9% saline twice daily and were challenged with naloxone on day 5. Nociceptive measurements using the 50°C tail immersion test were taken before and 30 min after each morphine injection, normalized to daily baseline measurement and presented as %MPE. After naloxone challenge, signs of withdrawal were recorded as previously described.[38,85] Jumping, teeth chattering, wet-dog shakes, headshakes, and grooming behaviors were evaluated at 5 min intervals for a total test period of 30 min, and a standardized score of 0 to 3 was assigned to each behavior. Allodynia, piloerection, salivation, ejaculation, and tremors/twitching were also evaluated, with one point given for the presence of the behavior during each 5-min interval. All signs were counted and compiled to yield a cumulative withdrawal score. Mice were weighed before and after naloxone challenge to calculate weight loss.

Plantar incision post-surgical model

Mice were maintained under light anesthetic with 1.5-2% isoflurane in oxygen (vol/vol) delivered via a nose cone. The hind paw was sterilized with iodine and ethanol, and a No. 11 blade was used to make a longitudinal incision approximately 5 mm long through the skin and fascia of the plantar hind paw beginning 2 mm from the proximal edge of the heel towards the toes, as described previously.[86] The underlying muscle was elevated with curved forceps. A single horizontal mattress suture was used to close the incision. Mechanical allodynia was assessed prior to incision (-24 h, 0 h) and at 2, 4, 6 and 24 h after incision using von Frey filaments (Ugo Basile), using the SUDO method as described by Bonin et al.[87] In a separate set of experiments, at 4 h post-incision, a morphine cumulative dose-response was performed to determine morphine potency (ED_{50}). Mice were given ascending doses (0.5, 1, 2.5, 5, 10, 15, 20 mg/kg) of morphine at 30-min intervals until paw withdrawal thresholds reached baseline levels. Thresholds were expressed as percentage of baselines to calculate ED_{50} values using a non-linear regression in GraphPad Prism (version 6) software.

Complete Freund's adjuvant (CFA) peripheral inflammation model

Male C57BL/6J mice were injected with CFA to induce mechanical allodynia. The plantar surface of the left hind paw was injected with 20 μL of CFA (Sigma, F5881).[88] Ro5 or vehicle was administered by intrathecal injection once per day for 3 days, as described above, beginning on the day of CFA injection. Ro5 was injected 30 min prior to CFA. To assess mechanical allodynia, the paw withdrawal threshold was determined with von Frey filaments (Ugo Basile), using the up-down method.[89] The baseline paw withdrawal threshold was assessed prior to Ro5 and CFA injection. A morphine cumulative dose-response was performed 2 h after the final Ro5 injection (2 days after CFA injection) to determine morphine potency (ED_{50}). Mice were given ascending doses (0, 1, 5, 10, 15 mg/kg) of morphine by intraperitoneal injection at 30 min intervals until the paw withdrawal threshold reached baseline level. The paw

withdrawal threshold was measured 30 min after each morphine injection. Thresholds were expressed as a percentage of baseline to calculate ED_{50} values using a non-linear regression in GraphPad Prism (version 10) software.

Spared nerve injury model

Spared nerve injury (SNI) surgery was performed on vehicle- and tamoxifen-treated male and female *Cx3cr1*-Cre^{ERT2}::*Runx1*$^{flx/flx}$ mice. Tamoxifen was administered as described above, and SNI surgery was conducted 28 days after the final tamoxifen injection.[90,91] Mice were anesthetized with isoflurane [5% in oxygen (vol/vol) for induction; 1.5% for maintenance]. The sciatic nerve was exposed via blunt dissection through the biceps femoris muscle of the left hind leg. The tibial and common peroneal branches of the sciatic nerve were ligated with Prolene suture (Ethicon, W8761) and transected distal to the site of ligation. The sural branch of the sciatic nerve was left intact. The muscle and skin were closed with Vicryl suture (Ethicon, J488G). To assess mechanical allodynia, the paw withdrawal threshold was determined with von Frey filaments (Ugo Basile), using the up-down method.[89] The baseline paw withdrawal threshold was assessed prior to SNI. A morphine cumulative dose-response was performed on day 7 post-SNI to determine morphine potency (ED_{50}). Mice were given ascending doses (0, 1, 5, 10, 15, 20 mg/kg) of morphine by intraperitoneal injection at 30 min intervals until the paw withdrawal threshold reached baseline level. The paw withdrawal threshold was measured 30 min after each morphine injection. Thresholds were expressed as a percentage of baseline to calculate ED_{50} values using a non-linear regression in GraphPad Prism (version 10) software.

Protein assessment

Immunohistochemistry

Rats and mice were anesthetized with pentobarbital (Bimeda-MTC Animal Health Inc., Cambridge, ON, Canada) or isoflurane (Fresenius Kabi, Germany) and perfused transcardially with PBS. Animals were then perfused with 10% formalin (wt/vol). Spinal cords were collected by hydraulic extrusion and post-fixed overnight in 10% formalin or 4% paraformaldehyde (PFA). On the next day cords were transferred to 30% sucrose, then embedded in OCT and stored at -80°C. For imaging, the lumbar segment was sectioned at 30 μm thickness using a cryostat. A subset of tissue was embedded in paraffin without sucrose and was sliced on a microtome at 10 μm thickness onto Histobond slides for staining. Free-floating or mounted spinal cord sections were incubated overnight at 4°C with one or more of the following primary antibodies: mouse anti-rat CD11b (clone OX-42,1:150, EMD Millipore, CBL1512, RRID: AB_93253), rat anti-mouse CD11b (clone M1/70,1:200, Abcam, ab8878, RRID: AB_306831), rabbit anti-Runx1 (clone EPR3099, 1:200, Abcam, ab92336, RRID: AB_2049267), rabbit anti-Ki67 (clone SP6, 1:500, Abcam, ab16667, RRID: AB_302459), rabbit anti-Iba1 (Wako, 1:1000, 019-19741, RRID: AB_839504). After washing in PBS, sections were incubated at room temperature (RT) with the appropriate fluorochrome-conjugated secondary antibodies: Cy3-conjugated AffiniPure donkey anti-mouse IgG (1:1000, Jackson ImmunoResearch, West Grove, PA, USA), Cy5-conjugated AffiniPure donkey anti-rabbit, and Alexa Fluor 555-conjugated donkey anti-rat IgG (1:1000, Abcam). Images were obtained using a Nikon Eclipse Ti C1Si Spectral Confocal microscope and a Nikon multiphoton A1R microscope. Images were acquired using EZC1 software (Nikon) or NIS-Elements (Nikon) software and converted using NIS-Elements imaging software. Quantification of immunoreactivity (IR) mean intensity and percent area positive labeling was performed using ImageJ (NIH).

Immunocytochemistry

Primary microglia were cultured on glass coverslips. Cells were washed with PBS, fixed in 4% PFA and permeabilized with 0.1% Triton X-100. Cells were blocked with 10% normal donkey serum (NDS) for 1 h at 4°C. Cells were incubated overnight at 4°C in PBS with 1% NDS and the following primary antibodies: mouse anti-rat CD11b (clone OX-42,1:500, EMD Millipore, CBL1512, RRID: AB_93253), rabbit anti-Ki67 (clone SP6, 1:500, Abcam, ab16667, RRID: AB_302459). After overnight incubation, cells were washed with PBS and incubated with secondary antibodies for 1.5 h at RT: Cy3-, and Cy5-conjugated AffiniPure donkey anti-mouse and anti-rabbit IgG, respectively (1:1000, Jackson ImmunoResearch). For human cultured microglia, cells were incubated for 1 h in blocking solution (5% NDS, 1% BSA, 0.1% Triton X-100 in PBS) and incubated overnight with rabbit anti-Runx1 (clone EPR3099, 1:200, Abcam, ab92336, RRID: AB_2049267) along with one of the following primary antibodies: rat anti-F4/80 (clone CI:A3-1, 1:200, Abcam, ab6640, RRID: AB_1140040), mouse anti-CD68 (clone ED1, 1:50, Abcam, ab31630, RRID: AB_1141557), mouse anti-CD45 (1:25, Abcam, ab65274, RRID: AB_1140876). Cells were washed with PBS and incubated with the appropriate secondary antibodies for 1 h: Alexa Fluor 555-conjugated donkey anti-rabbit (Life Technologies, A31572), Alexa Fluor 488-conjugated donkey anti-mouse (Life Technologies, A21202), Alexa Fluor 488-conjugated goat anti-rat (Life Technologies, A11006). Slides were imaged using a Nikon Eclipse Ti C1Si Spectral Confocal Microscope or Nikon multiphoton A1R microscope using NIS-Elements imaging software.

Multiplex cytokine assay

BV2 cell samples were treated and collected as previously described. Cell lysates and/or supernatants were sent to Eve Technologies (Calgary, AB, Canada) for analysis. Samples were run on a multiplex array using antibody-coupled beads to detect a variety of unique targets. The samples were run on the mouse cytokine/chemokine array 31-plex in duplicate.

Western blotting

Microglia or BV2 cells in culture were harvested in 200 μL lysis buffer containing 50 mM Tris HCl, 150 mM NaCl, 10 mM EDTA, 0.1% Triton X-100, 5% glycerol, protease inhibitors, and phosphatase inhibitors. Rat and mouse spinal cord tissue was rapidly isolated and homogenized in RIPA buffer containing 50 mM Tris HCl, 150 mM NaCl, 2 mM EDTA, 0.1% SDS, 1% NP-40, 0.5% sodium deoxycholate, 1 mM Na_3VO_4, 1 U/ml aprotinin, 20 μg/ml leupeptin, and 20 μg/ml pepstatin A. Both microglia and spinal cord samples

were incubated on ice for 30 min prior to centrifugation at 12,000 rpm at 4°C for 30 min. DRGs were homogenized using a bullet blender (Next Advance) with SSB02 beads (Next Advance) and lysed in RIPA buffer (1% Igepal CA-630, 0.1% SDS, 0.5% sodium deoxycholate in PBS) with protease and phosphatase inhibitors (Thermo Fisher Scientific) for 45 min, and then centrifuged at 10,000 g for 10 min at 4°C.

Total protein was measured using a Bio-Rad RC DC Protein Assay Kit (Bio-Rad, Mississauga, ON, Canada) or Pierce BCA Protein Assay Kit (Thermo Scientific). Samples were heated at 95°C for 10 min in loading buffer (350 mM Tris, 30% glycerol, 1.6% SDS, 1.2% bromophenol blue, 6% β-mercaptoethanol), electrophoresed on a precast SDS gel (4-12% Tris-HCl, Bio-Rad) or on a 10% polyacrylamide gel, and transferred onto nitrocellulose membrane. The membrane was probed overnight with one or more of the following primary antibodies: rabbit anti-Runx1 (clone EPR3099, 1:500, Abcam, ab92336, RRID: AB_2049267), rabbit anti-PU.1 (1:1000, Cell Signaling Technology, 2266, RRID: AB_10692379), rabbit anti-μ-opioid receptor (1:500, Alomone Labs, AOR-011, RRID: AB_2040044), mouse anti-β-Actin (clone AC-74,1:2000, Sigma-Aldrich, A5316, RRID: AB_476743), rabbit β-Tubulin III (1:1000, Sigma-Aldrich, T2200, RRID: AB_262133). Membranes were washed in TBST (20 mM Tris, 137mM NaCl, 0.05% Tween 20) and incubated for 1 h at RT in fluorophore-conjugated secondary antibodies (anti-rabbit and anti-mouse conjugated IR Dyes, 1:5000, Mandel Scientific, Guelph, ON, Canada). Membranes were imaged and quantified using the LICOR Odyssey Clx Infrared Imaging System (Mandel Scientific). Band intensity was quantified using ImageJ, normalized to β-actin or β-tubulin, and expressed relative to control samples.

Electron microscopy

Spinal lumbar dorsal horn tissue from tamoxifen ($n = 5$) and vehicle injected animals ($n = 6$) was collected and processed for electron microscopy. Mice were anesthetized by intraperitoneal injection of sodium pentobarbital (80 mg/kg), followed by transcardial perfusion using 3.5% acrolein [diluted in phosphate buffer (PB): 100 mM at pH 7.4] and 4% PFA (diluted in PBS: 50 mM at pH 7.4). Coronal sections (50-μm thick) from the spinal cord were cut with a vibratome (Leica VT1000S) in ice-cold PBS and kept at -20°C in a cryoprotectant solution [20% (v/v) glycerol and 20% (v/v) ethylene glycol in PBS] until further experiments. Spinal cord sections were washed 3 ×10 min in PBS, quenched in 0.3% H_2O_2 diluted in PBS, and incubated 30 min in 0.1% $NaBH_4$ (diluted in PBS). The sections were then blocked for 1 h in 10% normal goat serum, 3% bovine serum albumin, and 0.01% Triton X-100, and incubated overnight in the primary antibody rabbit anti-Iba1 (1:1000, Wako, 019-19741, RRID: AB_839504). The following day, the sections were washed three times in tris-buffered saline (TBS, 50 mM, pH 7.4) and incubated for 90 min in the secondary antibody biotin-conjugated goat anti-rabbit (1:200, Jackson ImmunoResearch). The sections were placed for 1 h in avidin biotin solution (1:100 in TBS, Vector Laboratories, PK-6100) and developed with 0.05% diaminobenzidine and 0.015% H_2O_2 in Tris buffer (TB, 0.05 M, pH 8.0).

For the electron microscopy preparation, the sections were washed three times in PBS for 5 min and incubated for 30 min in 1% osmium tetroxide [Electron Microscopy Sciences (EMS), Pennsylvania, USA, 19190] in PB (100 mM, pH 7.4). After washing 3 × 5 min in PB, the sections were dehydrated in ascending concentrations of ethanol for 5 min each (2 × 35%, 50%, 70%, 80%, 90%, 3 × 100%) and washed 3 × 5 min with propylene oxide (Sigma-Aldrich, 110205-18L-C). The tissue sections were then embedded overnight in Durcupan resin (20 g component A, 20 g component B, 0.6 g component C, 0.4 g component D; Sigma Canada, Toronto, 44610). The following day, the resin-infiltrated brain sections were placed onto fluoropolymer films (ACLAR®, EMS, 50425-25) and kept at 55°C in a convection oven for 5 days to allow for resin polymerization. After resin polymerization, areas containing the spinal lumbar dorsal horn were excised from the fluoropolymer sheet and glued onto resin blocks for ultramicrotomy sectioning. Sections (70-nm thick) were cut using a Leica Ultracut UC7 ultramicrotome and placed on copper mesh grids for transmission electron microscopy imaging. In each animal, 8 to 12 microglial cells were imaged at 80 kV using a transmission electron microscope (FEI Tecnai Spirit G2) and imaged with a magnification of 6800× with a Hamamatsu ORCA-HR digital camera (10 MP).

Microglial cells were analyzed for their intracellular content and parenchymal interaction (for the ultrastructural description of each organelle and parenchymal interaction, see St-Pierre et al.[92,93]). The shape descriptors of the microglial cytoplasm were analyzed using ImageJ (area, circularity, aspect ratio, roundness, solidity). Circularity of microglia was calculated as follows: $4\pi \times [\text{Area}]/[\text{Perimeter}]^2$, with a value of 1.0 indicating a perfect circle. A value approaching 0 indicates an increasingly elongated shape. Values may not be valid for very small particles. For the intracellular content, the number of lipidic inclusions, lipid bodies, lipofuscin, lysosomes, autophagosomes, dilated and non-dilated endoplasmic reticulum, elongated mitochondria, altered mitochondria and non-altered mitochondria were identified based on previously defined ultrastructural criteria.[92,93] The extracellular digestion (membrane degraded in the extracellular space in direct contact with a microglia) and extracellular space pockets were also identified. For the parenchymal interaction, the number of direct contacts with axon terminals, dendritic spines and the full synapse (axon terminal, dendritic spine and synaptic cleft) were analyzed.

RNA assessment

Quantitative RT-PCR (qPCR)

Cells or tissue were treated as previously described and collected in TRIzol (Thermo Fisher Scientific). mRNA was extracted using phenol:chloroform and precipitated with isopropanol. Samples were washed once in 100% ethanol and then reconstituted in double-distilled H_2O. mRNA was converted to cDNA using reverse transcriptase (M-MLV, Invitrogen or Vilo IV, Thermo Fisher Scientific). For rodent samples, qPCR was run with 25 ng cDNA and Taq Platinum DNA polymerase (Invitrogen) or Bio-Rad supermix (Bio-Rad) and primer sequences shown in Table S2. PCR was run in the Applied Biosystems Step One Plus system using Sybr Green as the

detection agent. *Rplp1* (60S ribosomal protein Large P1) was used as the reference gene for mRNA expression. For human samples, gene expression assays were performed using specific Human TaqMan® probes (Thermo Fisher Scientific). mRNA amplification was done using the following parameters: 92°C for 10 min (initial denaturation) followed by 45 cycles of 95°C for 15 s (denaturing), 60°C for 60 s (annealing), 72°C for 30 s (extension), and 72°C for 10 min (final extension). Melt curve was verified alongside results to validate the specificity of the qPCR reactions. Data were analyzed using the comparative Ct method ($2^{\Delta\Delta Ct}$), as previously described.[94] In one experiment, the *Runx1* qPCR amplicon from FACS sorted microglia was run on an agarose DNA gel.

Fluorescent in situ *hybridization (RNAscope)*

In situ hybridization was performed using the RNAscope Singleplex assay [RNAscope 2.5 HD Assay-RED, Advanced Cell Diagnostics (ACD), California, USA]. Mice were perfused with PBS followed by 4% PFA as with immunostaining. Brains were removed and post-fixed with 4% PFA overnight. Spinal cords were next processed using a TP1020 Leica Tissue Processor (Leica Biosystems, Germany), dehydrated in 70% ethanol and embedded in paraffin. Slices were obtained at 10 μm and mounted directly onto Superfrost slides. Paraffin removal, pre-treatment and processing were performed using the standard RNAscope Singleplex protocol. Briefly, slides were baked at 60°C for 1 h, deparaffinized, treated with H_2O_2 at RT for 10 min, boiled in target retrieval solution for 15 min and permeabilized with protease for 30 min. Samples were then hybridized with the *Oprm1* probe (Mm-Oprm1, ACD, Cat# 315841) for 2 h at 40°C. Samples were also run with a negative control probe, in parallel. Slides were then washed and hybridized with amplifiers and visualized with Fast Red. All probes and solutions were purchased from ACD. Immediately after this process, slides were blocked with 10% NDS with 0.1% Triton X-100 in TBS for 30 min at RT and immunohistochemistry against Iba1 was performed as described. Finally, samples were incubated in DAPI (1:10,000, Sigma-Aldrich, D9542), then cover slipped with ProLong Gold Antifade Mountant (Invitrogen, P36934). Slides were imaged using a Leica TCS SP8 confocal microscope equipped with a white-light confocal laser and HyD detectors (63x/1.30 NA objective). The percentage of Iba1-positive cells co-labeled for *Oprm1* was quantified. A cell was defined as *Oprm1*-positive if at least two *Oprm1* puncta overlapped with the cell's DAPI-labeled nucleus. The negative control revealed negligible background and no quantifiable *Oprm1* signal.

qPCR of microglia-specific RNA

Spinal cords were collected from tamoxifen-treated microglia-specific RiboTag mice (*Cx3Cr1*-Cre^{ERT2}::*Rpl22*^{HA}). Approximately 28 days after the last tamoxifen injection, tissue was collected for RNA preparation as described previously.[95] Briefly, tissue was homogenized and incubated with anti-HA magnetic beads (Miltenyi Biotec) for 2 h at 4°C. Bead-bound RNA was recovered by magnet, washed and purified using an RNeasy Micro Kit (Qiagen). RNA quantity was measured using a NanoDrop1000 (Thermo Fisher Scientific), and RNA was reverse transcribed to cDNA using a QuantiTect reverse transcriptase kit (Qiagen). Transcripts were amplified using SYBR Green PCR master mix (BioRad) and primers (Table S2) using the Step One Plus RT-PCR system (Applied Biosciences). PCR products were visualized using agarose gel.

Cell isolation for FACS

To isolate adult mixed cells for fluorescence-activated cell sorting (FACS),[96] vehicle- and tamoxifen-treated *Cx3cr1*-Cre^{ERT2}::*Runx1*$^{flx/flx}$ mice were deeply anaesthetized with 4% isoflurane in oxygen (vol/vol) and perfused with phosphate buffered saline (PBS). The spinal cord was rapidly isolated by hydraulic extrusion and placed in Hank's Balanced Salt Solution (HBSS). Spinal cords were cut into smaller sections and then transferred to a 70 μm cell strainer in DMEM supplemented with 2% FBS and 10 mM HEPES. In a subset of experiments where cells were prepared for single-cell sequencing, tissue was digested using 2 mg/mL collagenase for 1 h at 37°C. To deplete myelin, tissue was filtered through the strainer, mixed with isotonic Percoll, and Percoll (density 1.08) was underlain before centrifugation (1200 g, 20°C, 30 min). Cells accumulating at the interface between layers were removed, rinsed and stained for flow cytometry. Microglia were identified based on double-labelling of endogenous EYFP and CD11b-PE (clone OX-42,1:100, Thermo Fisher Scientific, 12-0110-82, RRID: AB_11150971) immuno-labeling. Sorted microglia were collected for qPCR and single-cell sequencing.

Single-cell transcriptional profiling

Single-cell transcriptomics was performed on FACS-purified microglia from spinal cords collected from *Cx3cr1*-Cre^{ERT2}::*Runx1*$^{flx/flx}$ male mice treated with vehicle or tamoxifen. Isolation of cells for FACS was performed as described above. Following FACS, both samples (vehicle- vs. tamoxifen-treated) were prepared in parallel using 10x Chromium's v2 chemistry (as described in Stratton et al.[97]). Briefly, the 10x™ GemCode™ Technology partitions thousands of cells into nanoliter-scale Gel Bead-In-Emulsions (GEMs). All cDNA generated from an individual cell shares a common 16 bp 10x barcode and a 10 bp Unique Molecular Identifier (UMI) to identify PCR duplicates. Quality control and quantification was performed using a TapeStation D1000 ScreenTape (Agilent Technologies). Sequencing was performed using an Illumina HiSeq 4000 (read 1 - 28 cycles, i7 Index - 8 cycles, read 2 - 91 cycles). Raw reads were processed using the CellRanger 2.1.0 pipeline with recommended parameters[98] where FASTQs were aligned to the mouse mm10 reference genome using the STAR algorithm. Each sample was sequenced to an average depth of 549 million post-normalized reads (76,443 reads per cell), and both samples were aggregated using mapped depth normalization to ensure equal number of confidently mapped reads per cell in both samples to a total of 7,186 barcoded cells. Filtered gene-barcode matrices were generated for both samples by counting UMIs and excluding non-cell associated barcodes. This output was then imported into Seurat (version 2.3.4) R toolkit for quality control and downstream analysis.[99] All functions were run with default parameters, unless specified otherwise. Low-quality cells (<400 genes, genes detected in <3 cells) were excluded from downstream analysis. Gene

Please cite this article in press as: Leduc-Pessah et al., Runx1 transcription factor modulates opioid analgesia and withdrawal in humans and rodents, Neuron (2025), https://doi.org/10.1016/j.neuron.2025.11.018

expression was log normalized to a scale factor of 10,000. UMI counts, gene counts, and percentage of mitochondrial genes detected in single cell data were plotted to determine outliers. Total gene and UMI counts were also plotted. Significant principal components were determined (PCs 1 through 15) using Elbow plots and by visualizing heatmaps. Graph-based clustering (at res = 0.6) using 1,358 highly variable genes were projected onto a tSNE plot to explore cell clustering.

Chromatin immunoprecipitation sequencing

Spinal cords were isolated from male C57BL/6J mice, as described previously. Tissue was disaggregated using a dounce homogenizer, and cell debris was removed by density gradient centrifugation with debris removal solution (Miltenyi Biotec, 130-109-398). Cells from 5 spinal cords were pooled, resuspended in 1 ml of PBS (with protease inhibitors) and crosslinked by addition of formaldehyde (final concentration of 1%) for 10 min at RT. Crosslinking was halted by addition of glycine, and cells were washed twice with ice-cold PBS, then processed for chromatin immunoprecipitation (ChIP) using the SimpleChIP Enzymatic Chromatin IP Kit (Cell Signaling Technology, 9003), following the manufacturer's instructions. Briefly, for each sample containing cells from 5 spinal cords, nuclei were prepared, and chromatin was digested by incubation with the provided micrococcal nuclease enzyme, diluted 1/5 relative to the manufacturer's recommendation. A probe sonicator (VC-40, Sonics & Materials, Inc.) was used to lyse the nuclei, using three 20-s pulses (output: 30; probe diameter: 3/16") interspersed with 30 s incubations on ice. Lysates were centrifuged at 9,400 g for 10 min at 4°C, and the supernatant (chromatin) was collected. DNA fragment size of approximately 150-900 bp was verified by gel electrophoresis, and concentration was determined using a NanoDrop spectrophotometer.

For each immunoprecipitation, chromatin from 10 spinal cords was pooled, yielding a sample of approximately 10 μg, and incubated with 9 μg of antibody against Runx1 (rabbit polyclonal, Abcam, ab23980) overnight at 4°C with rotation. Samples were then incubated with protein G magnetic beads for an additional 2 h at 4°C with rotation. Beads were pelleted using a magnetic separation rack and washed four times, after which chromatin was eluted from the beads by gentle mixing (1,200 RPM) in elution buffer at 65°C for 30 min. Crosslinking was reversed by adding proteinase K and incubating at 65°C for an additional 2 h. ChIP DNA was then purified using DNA purification columns (Cell Signaling Technology, 9003).

Three biological replicates were sequenced. For each replicate, ChIP DNA from 10-20 spinal cords was pooled. ChIP-seq library preparation and sequencing reactions were conducted by GENEWIZ, Inc./Azenta US, Inc. (South Plainfield, NJ, USA). ChIP DNA samples were quantified using a Qubit 2.0 Fluorometer (Life Technologies, Carlsbad, CA, USA), and the DNA integrity was checked with a 4200 TapeStation (Agilent Technologies, Palo Alto, CA, USA). An NEBNext Ultra DNA Library Preparation Kit (New England Biolabs, E7370L) was used, following the manufacturer's recommendations. Briefly, the ChIP DNA was end repaired and adapters were ligated after adenylation of the 3′ ends. Adapter-ligated DNA was size selected, followed by clean up and limited cycle PCR enrichment. The ChIP library was validated using a TapeStation and quantified using a Qubit 2.0 Fluorometer.

The sequencing libraries were multiplexed and clustered on one lane of a flowcell. After clustering, the flowcell was loaded on an Illumina Novaseq instrument according to the manufacturer's instructions (Illumina, San Diego, CA, USA). Sequencing was performed using a 2x150 Paired End configuration. Image analysis and base calling were conducted by the Novaseq Control Software. Raw sequence data (.bcl files) generated from the Illumina instrument were converted into fastq files and de-multiplexed using Illumina's bcl2fastq 2.17 software. One mis-match was allowed for index sequence identification.

The raw data for each sample were trimmed using Trimmomatic v0.38, and quality was assessed via FastQC. Cleaned reads were then aligned to the reference genome GRCm38 using bowtie2. Aligned reads were filtered using samtools 1.9 to keep alignments that (i) had a minimum mapping quality of 30, (ii) were aligned concordantly, and (iii) were the primary-called alignments. PCR or optical duplicates were marked using Picard 2.18.26 and removed. Prior to peak calling, reads mapping to mitochondria were called and filtered and reads mapping to unplaced contigs were removed. MACS2 2.1.2 was used for peak calling to identify open chromatin regions. If a blacklist of artefactual regions (areas with extremely high or low-mappability) was available for the provided reference genome, called peaks were filtered for these regions to mitigate errors due to mappability. From the three replicates, 451, 1641, and 13,194 peaks were identified. Valid peaks from the replicates were merged, such that only the peaks that were called in at least two out of the three replicates were kept for downstream analyses, resulting in 1529 peaks across 1406 genes.

Chromatin immunoprecipitation qPCR

Rat primary microglia cultures were generated as previously described. Cells were collected and processed following the manufacturer's instructions for the SimpleChIP Enzymatic Chromatin IP Kit (Cell Signaling Technology, 9003). Briefly, cells were fixed by adding formaldehyde (final concentration of 1%) to the media for 10 min at RT. Crosslinking was halted by addition of glycine, and cells were washed twice with ice-cold PBS, then scraped in ice-cold PBS containing protease inhibitor cocktail. Nuclei were prepared, and chromatin was digested by incubation with the provided micrococcal nuclease enzyme, diluted 1/2.5 relative to the manufacturer's recommendation. Nuclei were lysed and chromatin was collected, as described for ChIP-seq. For each immunoprecipitation, 5 μg of chromatin from morphine- or saline-treated microglia was incubated with 5 μg of antibody against Runx1 (rabbit polyclonal, ab23980, Abcam) or 5 μg of normal rabbit IgG (included with the kit) overnight at 4°C with rotation. Further processing of samples was performed as described for ChIP-seq, resulting in purified ChIP DNA samples.

The DNA sequences corresponding to the gene fragments of interest immunoprecipitated from mouse spinal cord cells in the ChIP-seq analysis were downloaded from the NIH Genome Data Viewer from *Mus musculus* (assembly GRCm38.p6) and subsequently used to blast search against the *Rattus norvegicus* whole genome sequence (assembly GRCr8) to identify the corresponding

Please cite this article in press as: Leduc-Pessah et al., Runx1 transcription factor modulates opioid analgesia and withdrawal in humans and rodents, Neuron (2025), https://doi.org/10.1016/j.neuron.2025.11.018

sequence on the rat genome and furthermore confirm it to be in proximity to the identified target gene. Primer sequences (Table S3) were designed using the Primer3 webtool set to generate a 100-200 bp amplicon and ordered for synthesis from Integrated DNA Technologies. Real time qPCR on either 2% input chromatin, Runx1 antibody immunoprecipitated chromatin, or IgG control chromatin was performed using an Applied Biosystems Quantstudio3 real time PCR system and PowerUP SYBR Green PCR Master Mix, according to the manufacturer's instructions. Primer pairs were validated by running real time qPCR with serially diluted input chromatin, confirming dilutional linearity and yielding efficiency values ranging from ~80-110%. PCR specificity was confirmed using melt curve analysis at the end of every qPCR experiment. Data for individual experiments were analyzed using QuantStudio Design & Analysis software (version 2.6.0), and quantities of target DNA amplified in Runx1 or IgG immunoprecipitated samples were normalized against the quantity in the 2% input samples.

Spinal cord electrophysiology recordings

Preparation of acute spinal cord slices

Parasagittal spinal cord slices were obtained from adult male mice (4 to 5 months old, *Cx3cr1*-Cre^{ERT2}::*Runx1*$^{flx/flx}$ mice treated with either tamoxifen or vehicle). Animals were anesthetized with 30% urethane (10 ml/kg) and subjected to a total laminectomy for the removal of the lumbar spinal cord, after which they were killed by cervical dislocation. The spinal cord was rapidly immersed in ice-cold oxygenated (95% O_2, 5% CO_2) NMDG-ACSF solution containing the following (in mM): 93 NMDG, 2.5 KCl, 1.2 NaH_2PO_4, 30 $NaHCO_3$, 20 HEPES, 25 Glucose, 5 Sodium Ascorbate, 2 Thiourea, 3 Sodium Pyruvate, 10 $MgSO_4$ and 0.5 $CaCl_2$. The dorsal and ventral roots were removed, and 300 μm-thick parasagittal slices were obtained with a vibratome (Leica VT1200S). Slices were allowed to recover for 15 min in NMDG-ACSF solution at 32°C and then for at least 45 min at RT in oxygenated holding ACSF solution containing (in mM): 92 NaCl, 2.5 KCl, 1.2 NaH_2PO_4, 30 $NaHCO_3$, 20 HEPES, 25 Glucose, 5 Sodium Ascorbate, 2 Thiourea, 3 Sodium Pyruvate, 2 $MgSO_4$ and 2 $CaCl_2$.[100]

Electrophysiology recordings

Patch pipettes were pulled from borosilicate glass capillaries (WPI) and filled with an intracellular solution containing the following (in mM): 130 $KMeSO_4$, 5 KCl, 2 $MgCl_2$, 10 Phosphocreatine-diNa, 10 HEPES, 0.5 EGTA, 4 ATP-diNa, 0.4 GTP-Tris; pH was adjusted to 7.2 with KOH, and osmolality ranged from 280 to 290 mOsm/kg (pipette resistance, 3 to 4 MΩ).

Slices were transferred to a recording chamber which was constantly perfused at 5 ml/min with oxygenated (95% O_2, 5% CO_2) ACSF composed of (in mM): 126 NaCl, 2.5 KCl, 2 $MgCl_2$, 2 $CaCl_2$, 1.25 NaH_2PO_4, 26 $NaHCO_3$, and 10 D-glucose; pH 7.35, 300 mOsm/kg. All recordings were made at 30-32°C. Neurons were visually identified with infrared differential interference contrast (IR-DIC) and 40x immersion objectives. LI was identified by visual inspection as a narrow dark band of gray matter with a typical reticulated appearance less than 50 μm away from the dorsal white matter, LII as a wider translucent band below LI.[101] Whole-cell voltage-clamp recordings were obtained from LI/LII neurons, and spontaneous excitatory postsynaptic currents (sEPSCs) were recorded at holding potential of -70 mV (corrected for measured junction potential). Data acquisition (filtered at 4 kHz and digitized at 10 kHz) was performed using a Multiclamp 700B amplifier and the Clampex 10.2 software (Molecular Devices). Access resistance was monitored during the recordings by applying a small hyperpolarizing voltage step (-5 mV) in between experimental epochs. Recordings were excluded from analysis if the access resistance changed by more than 20% or if it was greater than 20 MΩ.

Spontaneous excitatory postsynaptic currents

The recording of sEPSCs was divided in four experimental epochs as follows: a baseline of 10 min, a wash-in (of morphine) of 3-4 min, a morphine recording of 10 min, and a wash-out of variable length. The wash-in epoch started once the recording chamber was fully occupied by morphine (0.1 μM, Sigma-Aldrich). The washout epoch was not always present. Only cells with stationary sEPSC amplitudes and inter-event intervals, assessed by a *t* test on the slope of the respective parameter during the baseline recording, were considered for analysis. For this analysis, we selected from each cell (using MiniAnalysis software by Synaptosoft) at least 100 events from the ending section of the baseline recording and at least 100 events from the starting section of the morphine recording. We referred to this selection as the source set. For isolating the effect that morphine could exert on the amplitudes and inter-event intervals of sEPSC, we selected only those cells that responded to the drug treatment by either significantly increasing or decreasing these parameters according to a paired *t* test. Then, for each cell in each epoch (baseline and morphine), 50 events randomly selected from the source set were considered for further analysis. For the analysis of the cumulative distributions, we pooled the events of all cells per epoch.

Holding currents (I_h) were analysed in Clampfit 10.7 (Molecular Devices) in all cells that responded to morphine (see above). Any linear trend in this parameter, if present during the baseline, was subtracted from the whole experimental recording. Holding currents were estimated by averaging 30-60 s of the recordings (avoiding synaptic activity) as follows: baseline I_h, at the end of the epoch; morphine I_h, at the end of the first 5 min of the epoch. The change in holding current (ΔI_h) was calculated as morphine I_h – baseline I_h.

DRG electrophysiology recordings

DRG neurons were placed in a 1 ml chamber and perfused continuously at a rate of 1.5 ml/min with an extracellular solution containing (in mM): 140 NaCl, 5 KCl, 2 $CaCl_2$, 1 $MgCl_2$, 10 Hepes, and 10 D-glucose for current clamp recordings. Recordings were conducted at RT at 20x magnification using an inverted epi-fluorescence microscope (Olympus IX51, Olympus America Inc.). To identify IB4-positive neurons, coverslips were treated with IB4-FITC, a plant lectin conjugate, for 10 min. Whole-cell patch

clamp experiments were performed in both voltage-clamp and current-clamp modes using a software-controlled Axopatch 200B amplifier with a Digidata 1550A digitizer. Data were low pass filtered at 5 kHz and sampled at 10 kHz using Clampex 11 (all from Molecular Devices). Borosilicate glass pipettes were pulled and polished to a resistance of 2-3 MΩ with a DMZ-Universal Puller (Zeitz-Instruments GmbH). The patch pipettes contained (in mM): 105 K-gluconate, 30 KCl, 4 $MgCl_2$, 0.3 EGTA, 10 HEPES, 4 Na_2ATP, 0.3 Na_3GTP, and 10 Na-phosphocreatine at pH 7.35. All chemicals were procured from Sigma-Aldrich.

Under voltage clamp, cells were held at -70 mV, and membrane capacitance (Cm) and membrane resistance (Rm) were calculated in response to a -10 mV hyperpolarizing pulse using the Membrane Test function of Clampex. Resting membrane potential (Vm), rheobase (minimum current injection required to elicit an action potential), and resultant action potential amplitude of the neurons were evaluated by switching to current clamp before returning to voltage clamp control. Access resistance (Ra) and holding current (I_h) were monitored throughout the experiments to ensure recording stability, and recordings with unstable Ih or poor Ra (initial Ra > 20 MΩ or Ra > 10% change over the recording period) were excluded. Data were analyzed from recordings with 75-95% compensation to minimize offsets due to large voltage-clamp errors. Data analysis was performed using Clampfit 11 (Molecular Devices), Easy Electrophysiology (Easy Electrophysiology Ltd), and GraphPad Prism (version 10) software.

Post-operative analgesic use studies

Genotyping and linkage disequilibrium analysis

For SSRO subjects, whole-genome genotyping was performed using the Infinium assay II with an iScan system (Illumina, San Diego, CA, USA) according to the manufacturer's instructions after genomic DNA was extracted from whole-blood samples using standard procedures. The genotype data were evaluated as detailed in our previous report.[50] Briefly, the data for the whole-genome genotyped samples were analyzed using BeadStudio or GenomeStudio with Genotyping module v3.3.7 (Illumina) to evaluate the quality of the results. The genotype data from all five BeadChips were merged to analyze all of the samples simultaneously. A total of 295,036 SNP markers survived the filtration process and were used for the genome-wide association study.[50] Linkage disequilibrium (LD) analysis was then performed for 126 samples using Haploview v. 4.1.[72] For OAS subjects, total genomic DNA was extracted from peripheral blood or oral mucosa samples using standard procedures. The TaqMan allelic discrimination assay (Thermo Fisher Scientific, Carlsbad, CA) was used to genotype the rs2236431 SNP with a LightCycler 480 (Roche Diagnostics, Basel, Switzerland) and TaqMan SNP Genotyping Assays (Thermo Fisher Scientific) that contained sequence-specific forward and reverse primers to amplify the polymorphic sequence and two probes that were labeled with VIG and FAM™ dye to detect both alleles of the SNP (Assay ID: C___2184062_10), as described in previous reports.[102,103] To initially analyze SNPs within and around the *RUNX1* gene region, the genotype data for all of the SNP markers with *RUNX1* gene annotation were extracted among the entire genotype data for approximately 300,000 SNP markers that resulted from whole-genome genotyping in SSRO subjects. Of the 45 SNPs with minor allele frequencies above 0.001 that were located within the exon and intron regions and approximately within the 30 kbp 5′- and 3′-flanking regions of the *RUNX1* gene, SNPs for the association studies were selected among all of the extracted SNPs in SSRO subjects. To identify relationships between the SNPs that were used in the study, an LD analysis was performed for 126 samples among the entire 355 SSRO samples using Haploview v. 4.1.[72] To estimate the LD strength between the SNPs, the commonly used D' and r^2 values were pairwise calculated using the genotype dataset of each SNP. LD blocks were defined among the SNPs with minor allele frequencies above 0.05 that showed "strong LD" based on the default algorithm of Gabriel et al.,[104] in which the upper and lower 95% confidence limits on D′ for strong LD were set at 0.98 and 0.7, respectively. Tag SNPs in the LD block were consequently determined using the Tagger software package with default settings, which is incorporated in Haploview and has been detailed in a previous report.[105]

Comorbidity and Trauma Study

Genotyping and genotypic data cleaning

Genotyping of the CATS samples was performed using the Illumina Human660W-Quad BeadChip at the Johns Hopkins Center for Inherited Disease Research (CIDR). Details of genotypic data cleaning have been reported previously.[106] The current analyses used dosage data obtained via 1000 Genomes-based imputation.

QUANTIFICATION AND STATISTICAL ANALYSIS

General statistical analysis

All data are presented as the mean ± SEM, unless otherwise indicated. Tests of statistical difference were performed with GraphPad Prism (version 6) software, unless otherwise indicated, and details of the statistical testing are included in the figure legends. For all experiments, a criterion α level was set at 0.05.

Spinal cord electrophysiology recordings

Statistics

All statistical analysis was performed by custom-made scripts written in MATLAB 9.4.0 (The MathWorks Inc). We used *t* tests and paired *t* tests during the preprocessing of sEPSC as described above. We used the randomization cumulative residual entropy difference (RCRED) test (see below) for distribution-based analysis and Fisher's randomization test (section 6.2, Manly[107]) for

Please cite this article in press as: Leduc-Pessah et al., Runx1 transcription factor modulates opioid analgesia and withdrawal in humans and rodents, Neuron (2025), https://doi.org/10.1016/j.neuron.2025.11.018

location-based analysis (one-sample data and paired data). We set the number of permutations to 5000 for RCRED test and to 10000 for Fisher's randomization test, unless exhaustive (all possible) permutations were reached before those limits. Data points were deemed as outliers if they were more than 1.5 x IQR (interquartile range) above the third quartile or below the first quartile. All p values were adjusted for multiple comparisons by Hochberg's method.[108]

RCRED test

For the analysis of the cumulative distributions of sEPSC, we sought to design a randomization test sensitive to changes in dispersion due to morphine treatment. We chose the cumulative residual entropy (CRE), which can be interpreted as a measure of dispersion,[109] as the core of its test statistic. The details are as follows: For a nonnegative random variable X with complementary cumulative distribution function $\overline{F}(x) = 1 - P(X \leq x)$ its cumulative residual entropy (CRE) is defined as[110]:

$$\mathcal{E}(X) = -\int_0^\infty \overline{F}(x)\log\overline{F}(x)\,dx$$

We set X^A and X^B as the collection of measures of X under the experimental conditions A and B, respectively, and defined the test statistic $\tilde{T}$ as the studentized relative change in CRE of the transition from the condition A to the condition B:

$$\tilde{T} = \frac{T}{V^{1/2}} = \frac{\Delta\mathcal{E}(X)}{V^{1/2}} = \frac{1}{V^{1/2}}\,\frac{\mathcal{E}(X^B) - \mathcal{E}(X^A)}{\mathcal{E}(X^A)}$$

where $V^{1/2}$ is a non-parametric bootstrap estimator of the standard deviation of T[111] given by:

$$V^{1/2} = \frac{\widehat{T}^{*(0.9)} - \widehat{T}^{*(1-0.9)}}{2z^{(0.9)}}$$

where $\widehat{T}^{*(0.9)}$ is the 90th percentile of the bootstrap replications, and $z^{(0.9)}$ is the 90th percentile of a standard normal distribution. For the null hypothesis of no treatment effect the null reference distribution of $\tilde{T}$ was generated by randomly permuting X^A and X^B and exact p values were computed according to Phipson and Smyth [equation 2].[112]

We report the relative change in CRE, $\Delta\mathcal{E}(X)$, as a measure of effect size and assessed the difference between two of these effect sizes by the percentile bootstrap.[111]

Human genetic association studies

Post-operative analgesic use studies

Among the 355 subjects who underwent SSRO, one subject lacked postoperative clinical data, and two subjects lacked genotype data; thus, a total of 352 subjects were used for the analyses. In the present study, none of the clinically measured endpoints that were related to analgesic requirements (24 h postoperative fentanyl use and total perioperative analgesic use in SSRO subjects and frequency of rescue analgesics and fentanyl-converted total dose of rescue analgesics administered in OAS subjects) or pain scores (24 h postoperative VAS pain scores in SSRO subjects and NRS pain scores in OAS subjects) were normally distributed. Therefore, nonparametric analyses, including the Mann-Whitney U test and Kruskal-Wallis H test, were used to detect possible associations between the SNPs and clinical endpoints that were related to analgesic requirements or pain scores. In the analysis for SSRO subjects, postoperative fentanyl use during the first 24-h postoperative period (μg/kg), 24 h postoperatively assessed VAS pain scores (mm), and total perioperative analgesic use (converted to fentanyl dose [μg/kg]) were used as endpoint phenotypes related to opioid sensitivity. In the analysis for OAS subjects, highest NRS pain scores and the frequency and total dose of rescue analgesics (converted to fentanyl dose [μg/kg]) during the first 24-h postoperative period were used as endpoint phenotypes related to opioid sensitivity. To explore the association between the SNPs and endpoint phenotypes, both of trichotomized and dichotomized comparisons were performed between the genotypes by the Kruskal-Wallis H test and the Mann-Whitney U test for both subject groups. For these analyses, phenotypes and genotype data of each SNP were incorporated as dependent and independent variables, respectively. All of the statistical tests were performed using SPSS 25 software (International Business Machines Corporation, Armonk, NY, USA). The threshold for statistical significance was set at $p < 0.05$. In the initial analyses for SSRO subjects, the correction for multiple testing was performed using Bonferroni adjustments for the SNPs analyzed. The genotype distributions were checked using the χ^2 test, and the absence of significant deviation from the theoretical distribution that is expected from Hardy-Weinberg equilibrium was confirmed.

Comorbidity and Trauma Study

The mean value for opioid withdrawal symptom total endorsed by CATS EA cases was 12.0 (SD 3.5). Principal components analysis conducted using the SmartPCA program[113] generated five principal components (PCs) to include in the regression models as covariates to correct for admixture. Linear regression was performed using PLINK[114] with opioid withdrawal symptom total as the dependent variable and sex, age category, 5 PCs, and SNP dosage data as independent variables. Employing a LD threshold of $r^2 < 0.5$, the 3508 SNPs in the *RUNX1* gene that had adequate imputation were calculated to result in 772 independent tests. This value was used to determine Benjamini-Hochberg false discovery rate (FDR) corrected p values.[115]